

Fibrotic mechanism revealed by chemical screening  
combined with fascia explant assay

von Qing Yu

Inaugural-Dissertation zur Erlangung der Doktorwürde  
(Dr. med. vet.)  
der Tierärztlichen Fakultät der Ludwig-Maximilians-Universität München

Fibrotic mechanism revealed by chemical screening  
combined with fascia explant assay

von Qing Yu  
aus Hubei, P.R. China  
München 2020

Aus dem Veterinärwissenschaftlichen Department der Tierärztlichen  
Fakultät der Ludwig-Maximilians-Universität München

Lehrstuhl für Hygiene und Technologie der Milch

Arbeit angefertigt unter der Leitung von  
Univ.-Prof. Dr. Dr. h.c. Erwin Märtlbauer

Angefertigt in: Helmholtz Zentrum München  
Deutsches Forschungszentrum  
für Gesundheit und Umwelt (GmbH)  
Mentor: Dr. Yuval Rinkevich

**Gedruckt mit Genehmigung der Tierärztlichen Fakultät  
der Ludwig-Maximilians-Universität München**

**Dekan:** Univ.-Prof. Dr. Reinhard K. Straubinger, Ph.D.

**Berichterstatter:** Univ.-Prof. Dr. Dr. h.c. Erwin Märtlbauer

**Korreferent/en:** Univ.-Prof. Dr. Ralf S. Müller

**Tag der Promotion:** 25. Juli 2020

Für meine Familie

献给我的父母和家人

## Table of contents

Abbreviations .....	i
I. Introduction.....	1
1.1 Cutaneous wound healing.....	1
1.2 Pathological scarring and scarless healing.....	5
1.3 Introduction of fascia.....	10
1.4 Drug repositioning and screening strategies .....	15
II. Materials and methods .....	17
2.1 Mouse lines .....	17
2.2 <i>Ex vivo</i> skin explant assay.....	17
2.3 Prestwick chemical library® (PCL) and automatic screening of chemicals .....	18
2.4 <i>Ex vivo</i> fascia and dermis culture— suspension assay .....	19
2.5 <i>Ex vivo</i> fascia three-dimensional (3D) culture— fascia invasion assay.....	19
2.6 Invasion index and contraction index measurement.....	20
2.7 Histology .....	20
2.8 Cell culture .....	21
2.9 Immunohistochemistry .....	22
2.10 Immunocytochemistry.....	22
2.11 3D staining and whole mount imaging .....	23
2.12 Live imaging .....	24
2.13 Cell tracking.....	24
2.14 Data analysis .....	24
2.15 Statistics and reproducibility.....	25
III. Results .....	26
3.1 Characterization of the SCAD assay .....	26
3.2 Primary screening of 1280 chemicals with the SCAD assay .....	28
3.3 Development of dermis and fascia explant in suspension assay.....	33
3.4 Characterization of fascia invasion assay .....	34
3.5 Secondary screening- retest chemical hits in fascia invasion assay .....	39
3.6 Focal adhesion kinase (FAK) is unrelated to the inhibition of fascia migration .....	42
3.7 Microtubule organization is related to the inhibition of fascia cell migration.....	44
3.8 Hedgehog pathway is involved in the inhibition of fascia cell migration.....	45
IV. Discussion.....	49
4.1 3D culture in Matrigel.....	49
4.2 Fluvastatin and itraconazole for the treatment of fibrosis.....	50

---

## Table of contents

<b>4.3 Hedgehog pathway in fibrosis .....</b>	52
<b>V. Summary .....</b>	55
<b>5.1 Twenty-six hits were screened from PCL with SCAD assay .....</b>	55
<b>5.2 Establishment and characterization of a 3D fascia invasion assay .....</b>	55
<b>5.3 Two top scarring- inhibiting drugs were identified .....</b>	55
<b>VI. Zusammenfassung.....</b>	57
<b>5.1 Sechsundzwanzig Treffer wurden mit einem SCAD-Assay aus PCL gescreent .....</b>	57
<b>5.2 Erstellung und Charakterisierung eines 3D-Faszieninvasionsassays .....</b>	57
<b>5.2 Zwei Wirkstoffe mit Narben-hemmenden Eigenschaften wurden identifiziert.....</b>	57
<b>VII. References.....</b>	59
<b>VIII. Acknowledgement .....</b>	78

## Abbreviations

$\alpha$ SMA	$\alpha$ smooth muscle actin
ATC	Anatomical Therapeutic Chemical
CK1	Casein kinase 1
CK14	Cytokeratin 14
CCl <sub>4</sub>	Carbon tetrachloride
CD26	Cluster of differentiation 26
Col	Collagen
Ctrl	Control
CTGF	Connective tissue growth factor
DAPI	4,6-diamidino-2-phenylindole
DETC	Dendritic epidermal T cell
DMEM	Dulbecco's Modified Eagle Medium
D <sub>F</sub>	Fractal dimension
DHH	Desert Hedgehog
DLK1	Delta like non canonical notch ligand 1
DMSO	Dimethyl sulfoxide
DPP4	Dipeptidyl peptidase 4
EMA	European Medicines Agency
ECM	Extracellular matrix
EGF	Epithelial growth factors
EHS	Engelbreth-Holm-Swarm
<i>En1</i>	<i>Engrailed-1</i>

EPF	<i>Engrailed-1</i> positive fibroblast
F-actin	Filamentous actin
FAK	Focal adhesion kinase
FDA	Food and Drug Administration
FGF	Fibroblast growth factor
FN	Fibronectin
FPP	Farnesyl pyrophosphate
FSP1	Fibroblast specific protein 1
GFP	Green fluorescent protein
Gli1	Glioma-associated oncogene transcription factor 1
GPP	Geranyl pyrophosphate
GSK3 $\beta$	Glycogen synthase kinase 3 $\beta$
HGF	Hepatocyte growth factor
HH	Hedgehog
HMG-CoA	3-Hydroxy-3-methylglutaryl-coenzyme A
HUVEC	Human umbilical vein endothelial cell
IHH	Indian Hedgehog
IL	Interleukin
IP	Intraperitoneal
IPF	Idiopathic pulmonary fibrosis
IPP	Isopentenyl pyrophosphate
KGF	Keratinocyte growth factors
Ki 67	Antigen identified by monoclonal antibody Ki-67

---

Lac	Lacunarity
MMP	Matrix metalloproteinases
MOA	Mechanism of action
OCT	Optimal cutting temperature
PBS	Phosphate buffered saline
PCL	Prestwick chemical library®
PDGF	Platelet derived growth factor
PKA	Protein kinase A
P0	Post born day 0
PTCH	Patched protein
RT-PCR	Reverse transcription polymerase chain reaction
SCAD	Scar-in-a-dish
Smad	Fusion of <i>Caenorhabditis elegans</i> Sma genes and the <i>Drosophila</i> Mad (Mothers Against Decapentaplegic) genes
SMO	Smoothened
SHH	Sonic Hedgehog
Sca1	Stem cells antigen 1
Sufu	Suppressor of fused protein
TIMP	Tissue inhibitor of matrix metalloproteinase
TNF- $\alpha$	Tumour necrosis factor- $\alpha$
TGF $\beta$	Transforming growth factor $\beta$
VEGF	Vascular endothelial growth factor
3D	Three-dimension
4D	Four-dimension

# I. Introduction

## 1.1 Cutaneous wound healing

Skin is the largest organ of the human body that covers the whole organism. As part of the integumentary system, it provides a natural barrier to shield internal organs and tissues from various kinds of insults, such as ultraviolet light, chemical damage, and mechanical injury. Under physiological circumstances, the skin sustains an intrinsically self-renewal process during a lifetime. However, once the continuous structure of the skin is breached, a series of cell signalling cascades are triggered to prevent further damage, avoid potential infection, and rebuild new tissue. In classic view, cutaneous wound healing is divided into four overlapping but distinct stages- haemostasis, inflammation, proliferation, and tissue remodelling (Figure 1, Figure 2) [1, 2]. Each stage functions uniquely by certain types of cells and molecules that communicate the signals to orchestrate the spatio-temporal repair process.

The hemostasis response is originally provoked by the destruction of blood vessels that expose adventitia, the extracellular matrix (ECM) layer that adheres to the outer side of vessel endothelium [3]. The unveiling of damaged ECM initiates the coagulation cascade. Activated and degranulated platelets recruit and aggregate in the wound bed, interacting with the ECM proteins such as vitronectin, fibronectin, and thrombospondin and finally forming a fibrin clot that stops haemorrhage and blocks the infectious agents [4]. This fibrin clot also provides a basic matrix scaffold to facilitate migration of cells that are involved in the early healing phase. Platelets caged in the clot also release various kinds of cytokines and growth factors such as platelet derived growth factor (PDGF) and transforming growth factor  $\beta$  (TGF  $\beta$ ) into the surrounding wound environment. These factors make up the primary trigger to attract neutrophils and monocytes to the injury site to launch the inflammatory response [5].

In the inflammatory phase the first type of cells that infiltrate the injured site are neutrophils. They clear cell debris, phagocytose microorganisms and secret proteases to eliminate fragmented ECM, which facilitates the following phase of wound response, including cell migration and new ECM deposition [6]. Neutrophils also release various kinds of chemokines and growth factors such as PDGF and TGF  $\beta$  to

commandeer other inflammatory cells (such as monocytes), endothelial cells and fibroblasts into the injured site [6]. Generally, neutrophils are cleared up in the wound site by apoptosis or are phagocytosed by macrophages as soon as pathogens are eradicated from the injury site [7].

Following neutrophils, monocytes are the second inflammatory cell type that arrive at the injury site. These monocytes originate from the circulating system and differentiate into macrophages once they arrive at the wound site. The differentiated macrophages on one hand function immunologically by killing microbe intruders, clearing away crumbled matrix to smooth out the space for laying down granulation tissue in the next phase [8]. On the other hand, differentiated macrophages, accompanied by the skin resident macrophages release various cytokines, chemokines, enzymes and growth factors including interleukins 1 and 6 (IL-1 and IL-6), PDGF, vascular endothelial growth factor (VEGF), fibroblast growth factors (FGFs) superfamily, and TGF  $\beta$ , which subsequently facilitate tissue repair in the next proliferating phase [8-10].

The proliferation phase is predominated by angiogenesis, granulation tissue formation and re-epithelialization. Angiogenesis is critical for the healing process as the growing tissue at the wound site is lacking in nutrients and is under hypoxic conditions. Even though VEGF and FGF-2 are considered to be the common stimuli that trigger the neovascularization events, various kinds of cytokines and growth factors including hepatocyte growth factor (HGF), connective tissue growth factor (CTGF), VEGF and TGF  $\beta$ , as well as hypoxia, are considered to be promoting factors furnishing the capillary budding process [11-13]. Endothelial cells from vessels near the wound site are activated and secrete enzymes to lyse the basal membrane, sprout outside the vessels and at last form a new network of capillaries in the growing tissue [14]. The neovascularized system can then transport more oxygen and nutrients to the developing tissue and promote immune cell infiltration into the wound site to accelerate the healing process [14].

Fibroblasts are also recruited to the wound site by chemokines and growth factors (mainly PDGF and TGF  $\beta$ ) released in the previous inflammatory phase. They produce new ECM proteins including collagen III, fibronectin, proteoglycans, and hyaluronic

acid to refill the defect site [15, 16]. The loosely connected ECM scaffold intermingled with fibroblasts, macrophages and sprouted capillaries is termed as “granulation tissue” with a kind of soft and pink tissue-like appearance. Granulation tissue is fragile and can easily be traumatized. Fibroblasts are later activated into myofibroblasts that are characterized by the increased expression of alpha smooth muscle actin ( $\alpha$ -SMA) [17]. Myofibroblasts can generate contractile force through creating multiple pseudopods that attach to the surrounding ECM and then retract them. This kind of contractile force enables myofibroblasts to contract the wound, pulling wound edge together to minimize wound area [18].

Re-epithelialization initiates when the wound bed is filled up with granulation tissue, as keratinocytes need available tissue to attach and move across [19]. Keratinocytes that locate at the wound edge and in the epithelial stem cells reservoir in hair follicle bulge and interfollicular epidermis are the main contributors to the re-epithelialization process [20, 21]. Besides, epithelial stem cells from sweat glands and dedifferentiated sebaceous duct cells have also been reported to contribute to regenerating the epithelium [22, 23]. These keratinocytes or differentiated epithelial cells crawl from the wound edges and migrate along the surface of the granulation tissue, progressing in a sheet until the denuded territory is completely recovered. Growth factors such as epithelial growth factors (EGF) and keratinocyte growth factors (KGF) secreted by epithelial and non-epithelial cells have also been reported to promote the proliferation and migration of keratinocytes in this process [24]. Lastly, the newly formed epithelium layer undergoes stratification and differentiation to re-establish the squamous epidermal architecture that re-establish an intact skin.

In the remodelling phase granulation tissue is finally replaced by a mass of acellular and avascular matrix. The disorganized ECM produced during the proliferation phase is rearranged. In mature scar tissue, ECM fibres are aligned parallelly to each other, which is different from the basket-weave reticular pattern in normal skin tissue. ECM proteins produced in the former stage undergo certain changes that are controlled by matrix metalloproteinases (MMPs) and their inhibitors - tissue inhibitor of matrix metalloproteinases (TIMPs) [25]. Specifically, loosely structured collagen III transforms into more tense-resisted collagen I, in company with the declined content

of hyaluronan and the transition of glycosaminoglycans into more robust proteoglycan molecules [2, 26]. The remodelling phase may last for several weeks to years. During this phase, the newly formed tissue (normally a scar tissue) gradually gains increased strength and tensile strength but will never completely reach the level of the original uninjured tissue [27].

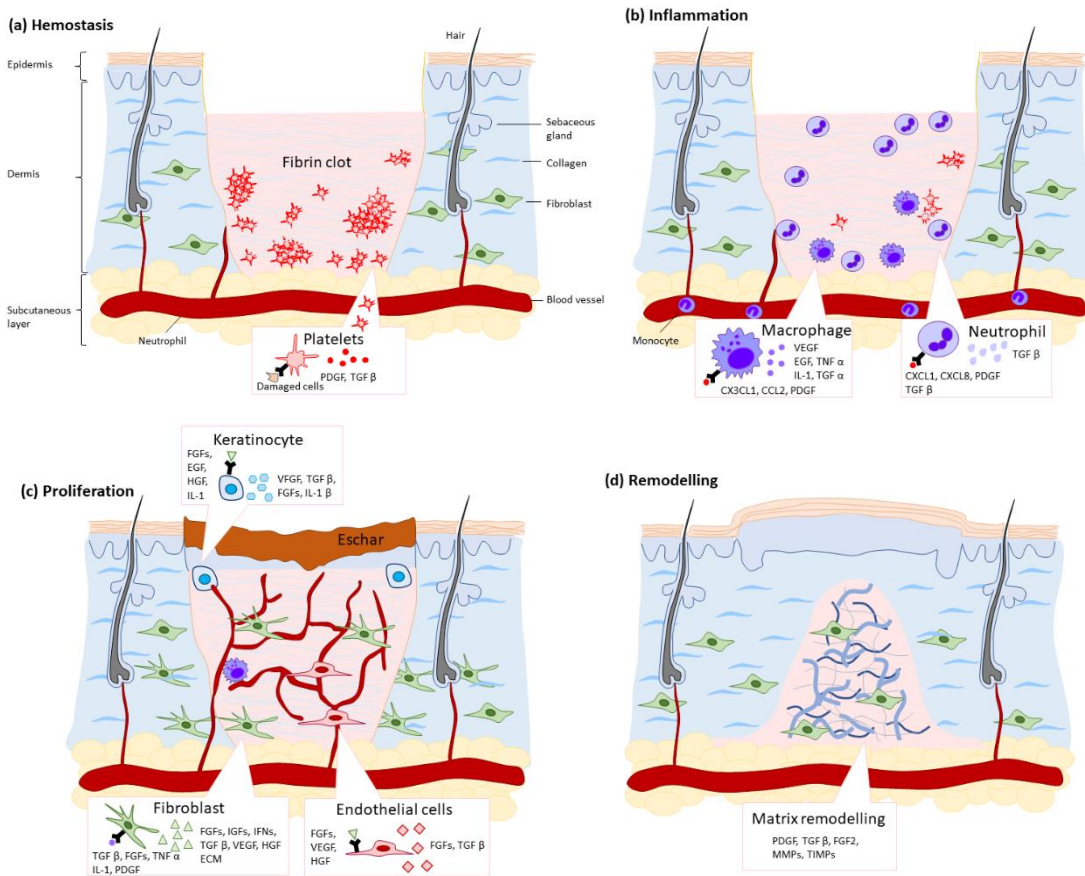


Figure 1. Four stages of skin wound healing. (a) In the hemostasis phase, platelets aggregate in the wound site and form fibrin clot to support cell migration. (b) In the inflammation phase macrophages and neutrophils attracted by PDGF and TGF  $\beta$  arrive later to phagocytose cell debris and external materials. (c) In the proliferation phase, fibroblasts are differentiated into myofibroblasts and deposit ECM; keratinocytes migrate along the granulation tissue to close the wound; endothelial cells are activated for angiogenesis. (d) At last, in the remodelling phase, growth factors and enzymes such as TGF  $\beta$ , PDGF, MMPs and TIMPs negotiate to transfer the previous fragile ECM into tense-resistant ECM (modified from Sun et.al., 2014) [2].

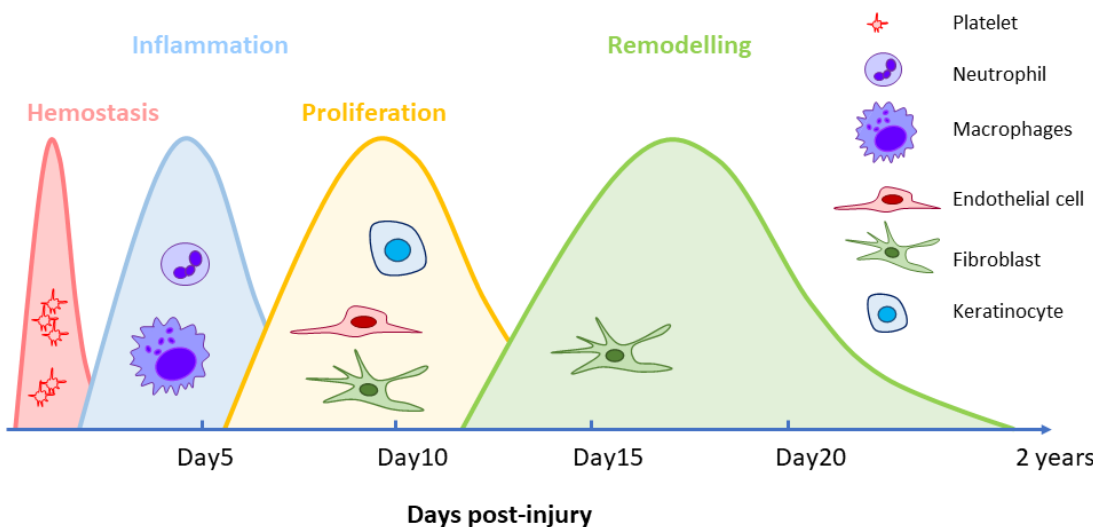


Figure 2. Timelines of wound healing processes. Hemostasis is triggered immediately after wounding to arrest bleeding. Inflammation begins within hours after wounding and may last for several days. The proliferation phase begins 5 to 14 days after wounding. In this phase, fibroblasts are attracted to the wound site; angiogenesis and re-epithelialization also occur during this phase. The remodelling phase already begins during the proliferation phase and could last for weeks to years (modified from Zomer, 2018) [28].

### 1.2 Pathological scarring and scarless healing

After injury, the innate surveillance system is intrinsically set off to reconstruct the integrity of tissue. This process leads to two extremely opposite results: tissue regeneration that forms an exact replica of the original tissue that regains most of the organ functions and physiologic performance; or scar formation that loses most of the function and physiologic performance. Whereas during fetal stages of development, injured skin may completely regenerate the original tissue architecture, this regenerative power is replaced at perinatal/postnatal life with scar tissue formation.

Moreover, any inability to activate, discontinue or dysregulate the wound healing phases can lead to a pathological and exuberant scar in adult skin. These scars are typically referred to as hypertrophic scars or keloids which are featured as overgrowth of scar tissue characterised by excessive production of ECM (Figure 3: bottom). Such pathological scars usually develop when the deep layers of skin are damaged, as superficial trauma to the skin in most cases does not lead to hypertrophic scars or keloids. The range and severity of excessive scarring has been divided into two main categories defined by Mancini and Peacock in the last century [29, 30]. According to their definitions, a hypertrophic scar appears as a rigid connective tissue that is elevated on the top of the skin but is restricted to the wound area, whereas a keloid

extends the fibrotic tissue mass beyond the wound site and invades the adjacent tissue [31]. The emergence of these two types of pathological scars can dramatically lower the quality of life and has psychological and physical effects caused by limited tissue/organ mobility, increased pain, and pruritus [32]. A hypertrophic scar is characterized as erythematous-based, pruritic fibrotic tissue that protrudes above the skin surface. The main cause of hypertrophic scars is surgical manipulations, with 40-70 % surgical operations leaving a hypertrophic scar. Burns are also a major trigger for hypertrophic scars, with a significant high incidence rate (around 91 %) in postburn wounds [33, 34]. Anatomically, hypertrophic scars usually develop in skin areas under tension such as neck and presternum or near knees and ankles [35, 36]. Once developed, hypertrophic scars grow rapidly at the early stage (up to 6 months) and then enter the remodelling phase, and regress over a few years into flattened scars [37]. In contrast, keloids are trapped in the proliferation phase and fail to progress into the remodelling phase of wound healing [38]. Keloidal scars may not degenerate after years and continue to undergo fibrotic growth similar to a benign tumour. Various kinds of insults can trigger keloid formation, including thermal injuries, surgical wounds, vaccinations, insect bites, infections, and endocrine dysregulation [39, 40]. Keloids mostly appear at anatomical sites that are devoid of hair follicles, such as upper part of the back, shoulders, earlobes and presternal skin [41, 42]. There is also a genetic susceptibility to keloid formation. Dark-skinned populations are found to be more prone to gain keloids than light-skinned populations, with an incidence rate of 6-16 % in African people [43].

The pathomechanisms of hypertrophic scar and keloid formation are not completely clarified yet. However, chronic inflammation and imbalance towards collagen synthesis over collagen degradation are thought to be the common paths of the pathogenesis. Some researchers take hypertrophic scars and keloids as an inflammatory dysregulation of the skin, in particular, dysregulation of the reticular dermis [40]. Pro-inflammatory cytokines including tumour necrosis factor- $\alpha$  (TNF-  $\alpha$ ), IL-1 $\alpha$ , IL-1 $\beta$ , and IL-6 are increased in keloids, which promote chronic inflammation and invasive growth of scarring tissue into the surroundings [44].

TGF  $\beta$  signalling is a key pathway that is involved in the formation of pathological scars at various stages such as fibroblast activation, ECM production and myofibroblast differentiation. Until now, at least 45 polypeptides have been discovered in the TGF  $\beta$  family, and the most representative members are TGF  $\beta$ 1, TGF  $\beta$ 2 and TGF  $\beta$ 3 [45]. TGF  $\beta$ 1 and TGF  $\beta$ 2 are reported to have a pro-scarring effect and TGF  $\beta$ 3 has an opposite anti-scarring effect. Robust expression of TGF  $\beta$  family ligands and their corresponding receptors have been detected in fibroblasts of hypertrophic scars after burn injury [46]. Increased mRNA expression of TGF  $\beta$ 1 and TGF  $\beta$ 2 are also found in fibroblasts from keloids, whereas TGF  $\beta$ 3 expression is dramatically decreased [47, 48]. In addition, TGF  $\beta$  up-regulates the expression of PDGF and VEGF in keloid-derived fibroblasts, which also favours fibroblast proliferation and ECM production [49, 50]. Pro-proliferative M2-type macrophages that stimulate fibroblast proliferation and collagen deposition in the proliferation phase of wound healing, are also abundant in keloids [51]. Overactive fibroblasts result in abnormal collagen synthesis of pathological scars, with a 7-fold increase in hypertrophic scars and an up to 20-fold increase in keloids, compared to that of normal skin tissue [52]. Histological analysis reveals that the main ECM in hypertrophic scars component is collagen III, which is normally present in the superficial dermis. In addition, hypertrophic scars are rich in nodules and extensive large collagen filaments. In contrast, keloids consist of thick collagen I and collagen III bundles with overactivated fibroblasts [53, 54]. A more detailed study characterizing the ECM composition of hypertrophic scars and keloids by reverse transcription polymerase chain reaction (RT-PCR) revealed that the expression of collagen I was approximately 3 to 4 times higher in hypertrophic scars and keloids and expression of hyaluronic acid was approximately 3 to 4 times lower than those in fetal tissues [55].

In contrast to the formation of pathological scars, many lower-form organisms in nature have developed regenerative abilities that act quickly to structurally repair wound tissues after injuries without scarring. Decades ago, scientists have noticed that an early fetal wound usually heals by regenerating and restoring the construction of the original skin tissue, rather than healing with a non-functional scar [56] (Figure 3 middle left). Specifically, the fetal dermis can lay down matrix proteins the same way

as the uninjured tissue. Furthermore, a higher level of hyaluronic acid is found in fetal skin tissues, compared to its equivalents in adults, which also promotes the regenerative restoration of skin structure [57, 58]. Interestingly, skin appendages such as hair follicles and sebaceous glands are also recreated in the healing fetal tissue [59]. Scarless healing is evolutionarily conserved in foetuses. Fetal scarless healing is not only restricted to humans but occurs also in many other mammals such as mice, rats, pigs, and monkeys [60, 61]. There are many factors that regulate wound healing towards a regenerative response. Studies have revealed that there was a low level of inflammation during the fetal wound healing process, suggesting that the absence of inflammation promotes rapid and impeccable healing of wounds [62]. This notion was further confirmed by Whitby, who observed a healing process towards development of scar tissue after inducing inflammation in fetal wounds [63]. Despite the alterations at the cellular level, cytokines at the molecular level also vary in fetal wounds. There is a low amount of pro-fibrosis growth factors including TGF  $\beta$ 1, TGF- $\beta$ 2 and PDGF, and a high amount of anti-fibrosis growth factors like TGF  $\beta$ 3 in fetal wounds [64]. Lastly, the high content of morphogenetic factors that engage in tissue growth and morphogenesis also contribute to a qualitative healing in foetuses that end in regeneration rather than scarring [64].

Not only the developmental stage plays a role in determining the healing consequences, but also the anatomic site. Scarless healing also exists in adult mammals. One example comes from the regenerative wound healing in oral mucosa. As compared to skin wounds, oral wounds often heal faster and result in a non-scar tissue that is almost identical to the original tissue (Figure 3 middle right) [65, 66]. Interestingly, oral cavity wound healing shares some characteristics with the fetal healing process that brings on a perfect healing. The gingival fibroblasts are able to contract the lattice matrix faster than their counterparts in dermis [67]; there is a prolonged release of TGF- $\beta$ 3 in oral wounds [68]; the saliva in the oral cavity provides a moisture environment and unique profiles of growth factors and cytokines, similar to the effect of the amniotic fluid in uterus that drives a qualitative healing process [69]. Moreover, investigations showed that there is less infiltration of macrophages,

neutrophils, and T cells in the oral wound, due to a low number of cytokines such as IL-6 and IL-8 that hamper the inflammatory reaction [70, 71].

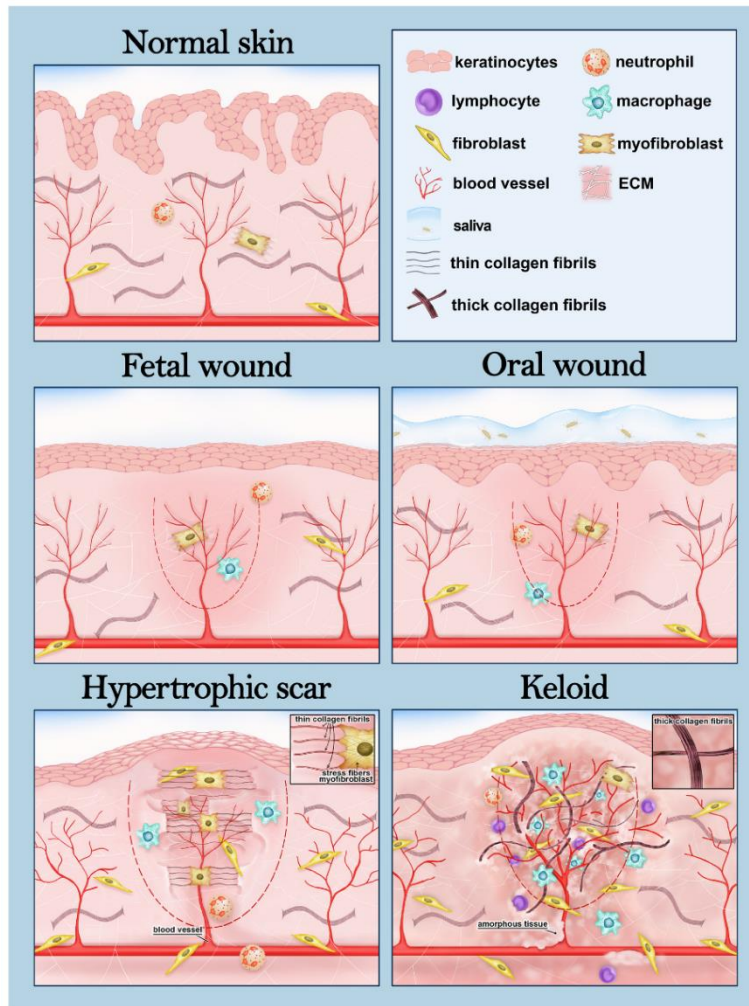


Figure 3. Schematic illustration of the structure of normal skin, two types of scarless healing and two types of pathological scars. Wound area is separated from the adjacent tissue by the dashed line. For scarless healing, fetal wound and oral wound share a debilitated inflammation response and similar skin structure as normal skin, demonstrated by the few macrophages and neutrophils in the wound bed without newly deposited ECM. In oral cavity, the humid environment also promotes the wound to heal scarlessly. For the two types of pathological scars, hypertrophic scar and keloid also share some characteristics, such as a high number of myofibroblasts, strengthened inflammation response and massive accumulated ECM. But in hypertrophic scar thin collagen fibres are aligned parallelly and the scar is restricted in the wound site. Whereas in keloid the scar tissue extends beyond the injury area and bulge above the skin, with disorganized ECM deposition and aggressive angiogenesis (Image is reproduced from Karppinen, 2019, with permission from F1000 Research) [44].

In the animal kingdom there are also cases of adult mammalian skin regeneration. For example, African spiny mice (genus *Acomys*), with outstanding repair and regeneration properties, represents a new model to study the evolutionary mechanisms that led to the loss of mammalian regeneration, and its replacement with scar tissue. On one hand, the relatively weak structure of the integumentary system of spiny mice makes it fragile and easy to break, which facilitates their escape from predators. On the other hand, the weak structured skin can quickly contract the wounds and regenerate the tissue (Figure 4) [72]. Notably, *Acomys* can fully regenerate the traumatized tissue after punch wounding in the ear, with de novo formation of hair follicles, sebaceous glands, cartilage, and adipose tissue [72, 73]. Until now, most studies still focus on the conventional murine model, far less research has been given to the new *Acomys* model organism, and further investigation is needed to uncover the mystery of their postnatal regenerative capacity.



Figure 4. African spiny mouse displays quick healing after injury. (a) One species of African spiny mouse- *Acomys kempi*. (b) Scab formation at post-injury day 3 of full-thickness wounding. (c) Wounding area is covered with newly formed spiny hairs at post-injury day 30 (Image is reproduced from Seifert, 2012, with permission from Springer Nature, license number: 4794160601934) [72].

### 1.3 Introduction of fascia

Fibroblasts are key players that not only produce and organize ECM in tissue but also interact with other cell types to orchestrate the dynamic wound healing process. With the various roles they play in a diversity of biological activities, fibroblasts are considered to be a heterogenous population consisting of distinct cell types. By conducting cell transplantation and lineage tracing experiments in mice, scientists have categorized fibroblast populations into two main classes on the basis of their surface expression and function, with papillary dermal fibroblasts expressing CD26<sup>+</sup>Sca1<sup>-</sup> in the upper dermis responsible for arrector pili and hair follicle formation, and reticular fibroblasts expressing Dlk1<sup>+</sup>Sca1<sup>-</sup> in the lower dermis accountable for

production of fibrillar ECM. When it comes to injury, the upper fibroblasts are recruited only for re-epithelialization, whereas the lower lineage cells are the contributors to the initial repair after wounding [75]. In 2015, Rinkevich et.al. identified a unique fibroblast lineage that is responsible for scar formation, namely *Engrailed-1* positive fibroblast (EPF), as this fibroblast population is positive for the homeobox transcription factor *Engrailed-1* during embryonic stages. By applying flow cytometry and surface marker screening panel, they determined CD26/ dipeptidyl peptidase-4 (DPP4) as the surface marker of EPFs. When inhibiting the CD26 positive cells with small molecular inhibitor, the wound healing process is delayed but it heals with almost no scar [76].

A recent scientific study has uncovered fascia as a major source of scar formation in deep wounds [77]. But what is fascia? According to the definition from the Fascia Nomenclature Committee (2014), “The fascial system consists of the three-dimensional continuum of soft, collagen containing, loose and dense fibrous connective tissues that permeate the body. It incorporates elements such as adipose tissue, adventitia and neurovascular sheaths, aponeuroses, deep and superficial fasciae, epineurium, joint capsules, ligaments, membranes, meninges, myofascial expansions, periosteum, retinacula, septa, tendons, visceral fasciae, and all the intramuscular and intermuscular connective tissues including endo-/peri-/epimysium. The fascial system interpenetrates and surrounds all organs, muscles, bones and nerve fibres, endowing the body with a functional structure, and providing an environment that enables all body systems to operate in an integrated manner.” [78] To be simplified, fascia is a sheet of connective tissue network that wraps the entire body, with fibroblasts, blood vessels, lymphatic tubes, adipose tissues, bones, cartilages, muscles, immune cells, and nerve systems integrated inside [78]. Collagen I and collagen III are the major ECM proteins that make up the supportive structure of fascia [79]. Besides, fascia tissue is also rich in hyaluronic acid that maintain the fluidic configuration and viscoelastic property of the tissue [80]. Among the various cell types resident in fascia, fibroblasts play a significant role in performing the fundamental functions of fascia such as tension transmission and tension resistance [81]. Fibroblasts can quickly flatten and spread out when fascia layer is extended by an

external force. This kind of morphological alteration on one hand assists fibroblasts to adapt themselves to the surroundings, on the other hand restrains the stress delivered to the deeper layers of the tissue [82]. In addition, fibroblasts are able to control and modulate ECM proteins to sustain the activity and integrity of fascia [83]. By secreting MMPs and TIMPs, the ECM synthesis and degradation in fascia are maintained in balance by fibroblasts [25].

Fascia tissue is important for our body to function properly and is firmly related to our general health. The motion ability of our body is mediated through fascia by allowing muscles to slide smoothly. Fascia can sense the mechanical stress from the external environment and transmit the force to intra- and extra-muscular tissues [84]. Fascia is not just a protective layer that holds the body together, it is also linked to many diseases occurring in the body. Pathological fascia containing numerous myofibroblasts can lead to clinical symptoms like Dupuytren's disease, Ledderhose's disease and frozen shoulder, due to the great contractile force produced inside [85-87]. Abundant nerve bundles distributed in fascia also relate to the pain sensation in patients. Relaxing fascial structures can relieve pain and increase mobility and muscle strength in patients diagnosed with patellar tendinopathy, chronic ankle sprain sequel and subacute whiplash disorder [88-90]. Table 1 gives a comprehensive view of the diseases caused by fascial dysfunctions [91].

Table 1. Various of diseases caused by dysfunctions of fascia

	Lack of stiffness	Increase of stiffness	Decreased shearing ability
Local	<ul style="list-style-type: none"> <li>• Inguinal hernia</li> <li>• Abdominal hernia</li> <li>• Lumbar hernia</li> </ul>	<ul style="list-style-type: none"> <li>• Dupuytren contracture</li> <li>• Frozen shoulder</li> <li>• Morbus Ledderhose</li> <li>• Hypertrophic scars</li> <li>• Peyronie's disease</li> <li>• Plantar fasciosis</li> </ul>	<ul style="list-style-type: none"> <li>• Nerve compression syndromes</li> <li>• Postsurgical abdominal adhesions</li> <li>• Chronic low back pain</li> </ul>
Global	<ul style="list-style-type: none"> <li>• Ehlers-Danlos syndrome</li> <li>• Marfan syndrome</li> <li>• Hypermobility syndrome</li> </ul>	<ul style="list-style-type: none"> <li>• Sclerodermia</li> <li>• Duchenne dystrophy</li> <li>• Spastic paresis</li> <li>• Major organ fibrosis</li> </ul>	

Table 1 is reproduced from Klingler, 2014 with permission from Springer Nature, license number: 4794180639079 [91].

In the wound healing field, many studies have previously focused on the function of fascia healing in abdominal wound repair. Failures in fascia healing after surgical celiotomy can be diagnosed only when hernias are identified, which not only cause sufferings for patients but also bring on huge economic loss in medical treatments [92]. It has been reported that fascia healing is important for successful abdominal wall restoration. The authors applied two different injury models to damage dermis and fascia, respectively, and found that fascia layer healed faster than dermis, with elevated fibroblast cellularity and collagen deposition, which finally resulted in fascial fibrosis [93]. *In vitro* cell culture experiments showed that, compared to their dermal counterparts, fascia fibroblasts exhibited superior cell proliferation ability and greater collagen compaction property, a distinguished phenotype that speeds up acute wound repair [94]. Surgeons also noticed that in clinical cases the standard subcutaneous suture method that stitches dermis and epidermis together could result in ischemia and multiply the chance to develop a hypertrophic scar. But this risk can be decreased when sutures were placed separately in deep fascia and superficial fascia to reduce tension force generated by fascia (Figure 5) [95, 96].

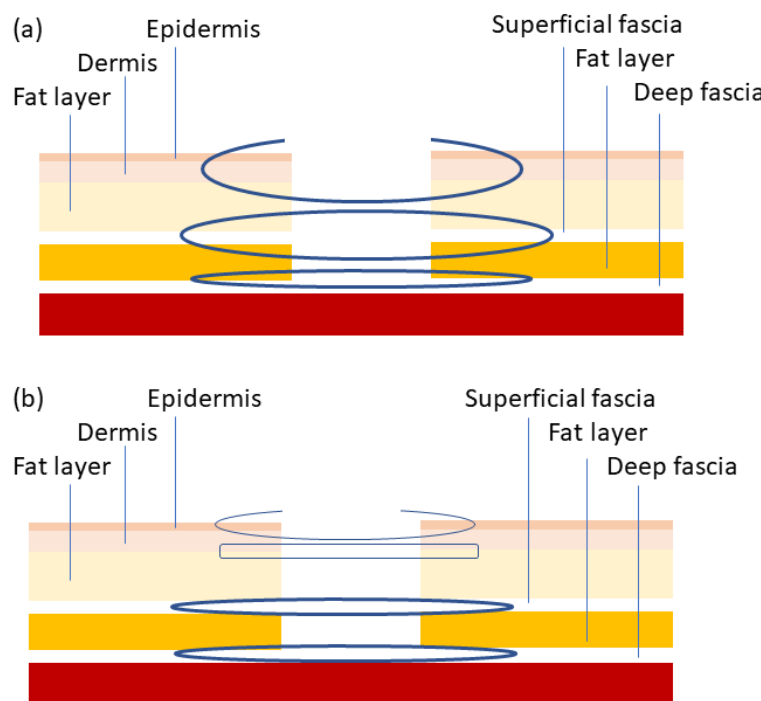


Figure 5. Standard subcutaneous suture (a) and fascia tension-reduced suture (b) (modified from Ogawa, 2011) [95].

Earlier studies were interested in defective fascia sliding that was affected by scarring and fibrosis. However, new findings linked fascia to wound healing and scar formation [77]. By transplanting murine fascia tissue and dermal tissue into immune-deficient mice separately, researchers found that fascia was the main contributor of scar formation in skin, rather than the classical view that regarded dermal fibroblast as the primary repair cells of wound healing. Further labelling of fascia tissue showed that fascia served as a mobile tissue that rapidly shifted to the defect area to fill the vacancy, alongside with the immune cells, vessels, lymphatic vessels, and nerves in the fascia tissue [77]. This new scientific discovery may give insights into further understanding of scar formation and wound healing, providing guidance to medical intervention for scarless repair.

Even though mouse (*Mus musculus*) is the most often used species in animal models to mimic the human wound healing and scar formation, there are anatomic differences between the construction of human skin and murine skin (Figure 6). Both human skin and murine skin share a three-layer structure - epidermis, dermis and the subcutis. However, human skin is much thicker and is tightly attached to the underlying tissues. Murine skin is relatively thin and loose, with a weaker adherence to the tissue beneath it [97, 98]. In addition, mouse back skin has a subcutaneous muscle layer under the hypodermis, anatomically named as panniculus carnosus muscle, which is unique to murine skin but minimally present or completely absent in human skin. This special muscle layer extends contractile force to skin and allows wound closure to occur more rapidly in murine wounds than in human wounds. In contrast, in humans wound closure is largely completed by granulation tissue formation and re-epithelialization [99, 100]. Interestingly, fascia location and distribution also differ across human and murine skin. In mouse skin fascia tissue is a separate layer situated between panniculus carnosus and the skeleton muscle and comprised of several layers of connective tissue with fibroblasts, immune cells, nerve bundles, vessels and lymphatic vessels spread inside. In human skin there are two layers of fascia tissues, namely superficial fascia and deep fascia respectively. Superficial fascia is beneath the first fat layer and deep fascia is located between the second fat layer and the underlying muscle tissue (Figure 6).

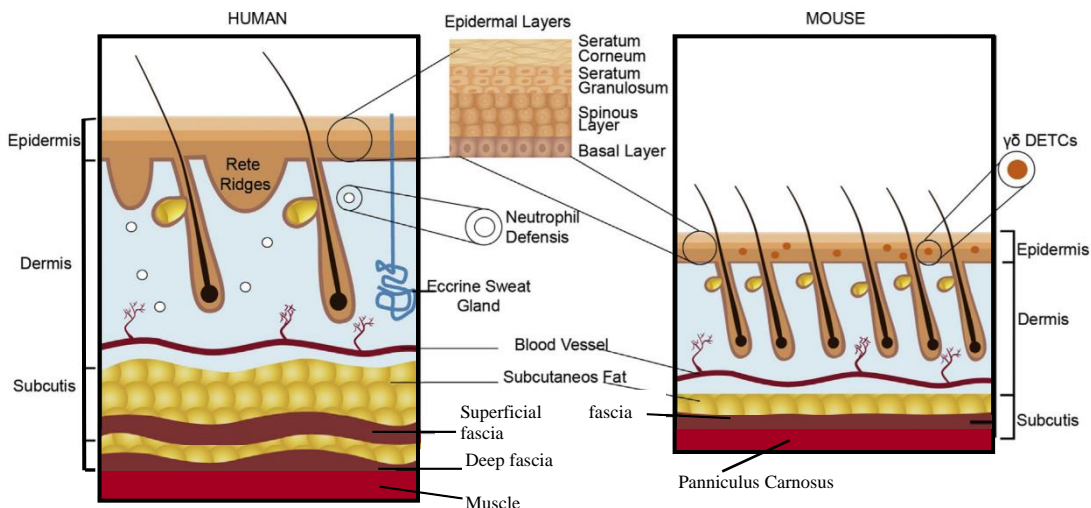


Figure 6. Architecture of human skin and murine skin. Human skin is much thicker than murine skin. In human skin, there are two layers of fascia- superficial fascia and deep fascia; whereas in murine skin there is only one fascia layer that is located between the panniculus carnosus and skeleton muscle (image is reproduced and modified from Zomer, 2018, with permission from Elsevier, license number: 4794160601934) [28].

#### 1.4 Drug repositioning and screening strategies

Drug development is a high-priced, long-term, laborious, and complex process. Usually, it takes more than 10 years to develop a single effective drug, from biomarker identification and validation to modification and optimization, and progress to clinical trials before finally entering the market [101]. Conventional drug discovery undergoes five phases including target identification, preclinical research, safety evaluation, clinical trials, Food and Drug Administration (FDA) review and security risk assessment from FDA after marketing (Figure 7) [102, 103]. The fact that putting a new drug into market takes long development times and demands numerous costs with high attrition rates leads to more attention to drug repositioning in pharmaceutical industry. The aim of drug repositioning is to find new therapeutic effects of approved drugs that have initially been out of scope for the new treatment purpose. Compared to the conventional drug discovery strategy, drug repositioning is more efficient, less costly and with higher success rates. It usually goes through four stages including target molecular discovery, chemical acquisition, clinical research, and FDA monitoring after marketing (Figure 7). The timeline of discovering a “new” drug for drug repositioning decreases to 8 years on average [104].

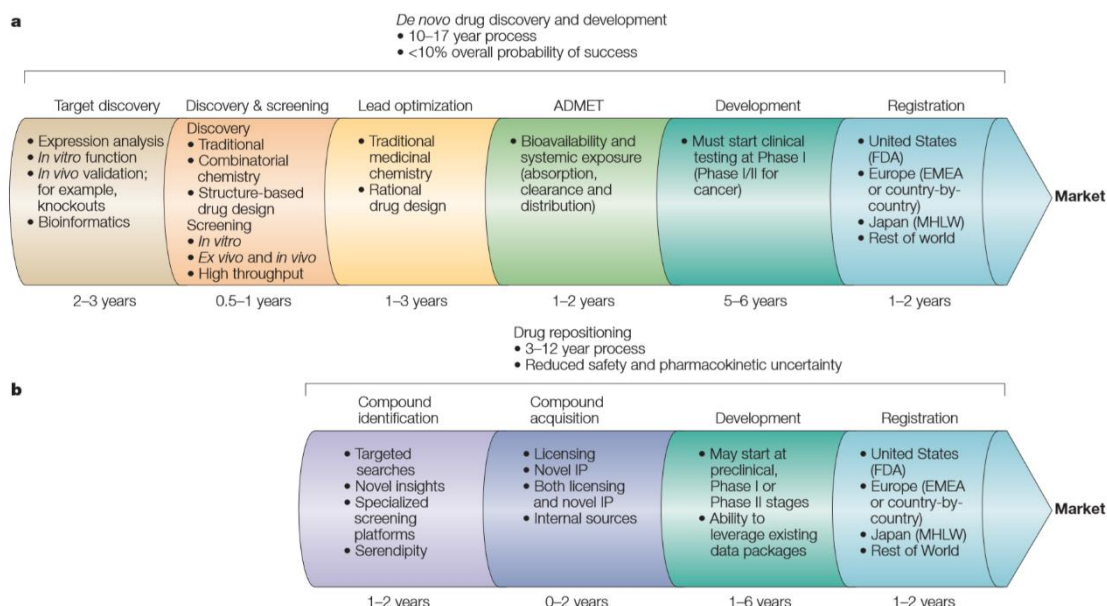


Figure 7. Schematic illustration of traditional drug discovery process (a) and drug-repositioning process (b) (image is reproduced from Ashburn, 2004, with permission from Springer Nature, license number: 4794171030385) [104]. ADMET, absorption, distribution, metabolism, excretion, and toxicity; EMEA, European Medicines Agency; FDA, Food and Drug Administration; IP, intellectual property; MHLW, Ministry of Health, Labour and Welfare.

Phenotypic screening is a classical strategy to repurpose existing approved drugs for new treatments in diseases. Phenotypic screening is based on the unbiased phenotypic measurements in biological contexts, such as cells, tissues, or animal models, with no concerns about the correlation between chemicals or molecular targets and the expected therapeutic effect. With known mechanism of action (MOA) and available clinical safety data of the old drugs, it takes less time and efforts to translate the altered phenotypes into new therapeutic targets [105]. It is reported that between 1999 and 2008, 28 first-in-class drugs approved by FDA were identified and developed through phenotypic screening [106]. Many drugs including the first anti-HIV drug and the first anti-tuberculosis drug were hits upon by phenotypic screening [107, 108].

## II. Materials and methods

### 2.1 Mouse lines

*En1<sup>cre</sup>; R26<sup>mTmG</sup>*, *En1<sup>cre</sup>; R26<sup>mCherry</sup>*, *C57BL/6J* were purchased from Charles River or Jackson laboratories or generated in Research Animal Facility at the Stanford University as previously described [76]. The *Engrailed-1 (En1)* gene is expressed in a small number of cells during embryogenetic stage. When the *En1<sup>cre</sup>* mouse is crossed with *R26<sup>mTmG</sup>*, Cre-Lox recombination will allow *En1* positive cells to be green in the cell membrane and *En1* negative cells to be red in cell membrane. When the *En1<sup>cre</sup>* mouse is crossed with *R26<sup>mCherry</sup>*, Cre-Lox recombination will allow *En1* positive cells to be mCherry in the cell nucleus and *En1* negative cells express no fluorochrome. Animals were housed in the Animal Facility at Helmholtz Zentrum München at constant temperature and humidity with a 12-hour light cycle. Food and water were provided ad libitum. All the tissues used in this thesis were collected as organ withdrawal after sacrificing the animals. All the experiments conducted in this thesis were done *ex vivo*.

### 2.2 *Ex vivo* skin explant assay

Post born Day 0 (P0) neonates of C57BL/6J wild type mice were first sacrificed by decapitation. Then dorsal back skin was isolated to make 2 mm full thickness biopsies ( $\varnothing$  2mm, Stiefel) that included the epidermis, dermis, and deep subcutaneous fascia layers. The whole skin tissue explant system is termed as scar-in-a-dish (SCAD) assay (Patent Application no. PLA17A13). The SCAD tissue was maintained in DMEM/F12 cell culture medium (Life Technologies) supplemented with 10 % FBS (Life Technologies), 1 % non-essential amino acid (Thermo Fisher), 1 % Glutamax (Thermo Fisher), 1 % penicillin and streptomycin (Thermo Fisher) in a 37 °C incubator supplied with 95 % O<sub>2</sub> and 5 % CO<sub>2</sub>. Medium was changed every other day until day 5 when SCADs were collected and fixed for histology analysis. Of note, the excised skin was submerged dermis-side up in culture media, which confined the scar-prone fibroblasts to the explant and discouraged their adherence to the tissue culture plate.

### **2.3 Prestwick chemical library® (PCL) and automatic screening of chemicals**

The Prestwick library contains 1280 approved small molecules approved by FDA, European Medicines Agency (EMA) or other agencies that covers a range of major anatomical therapeutic classes including central nervous system (19 %), cardiovascular system (11 %), metabolism (24 %) and infectious diseases (16 %). The purity of the compounds was > 90 % as reported by the provider of the compounds. The PCL provides an additional advantage as all chemicals are of stable physicochemical properties, show a high range of chemical diversity, and are with known bioavailability and safety data in humans. All this information helps to reduce the probability of screening low-quality hits and save the costs of preliminary screening process. More details about drug therapeutic category and drug targets are shown in Figure 8.

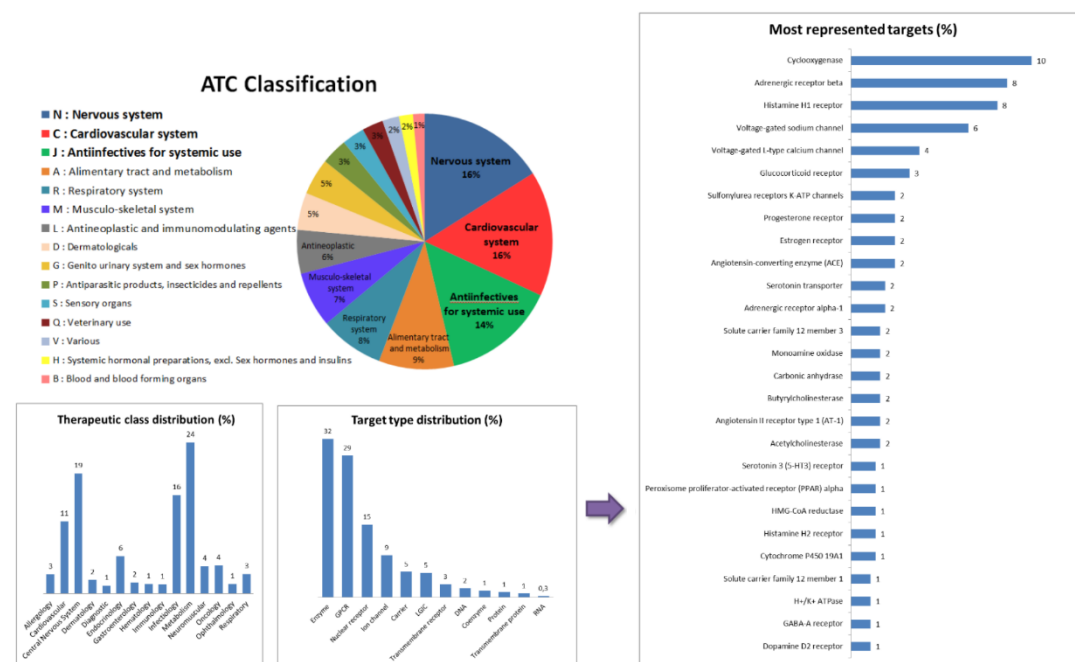


Figure 8. Anatomical Therapeutic Chemical (ATC) classification and target distribution of PCL [109] (Reproduced with permission obtained by Prestwich Chemical).

In order to accommodate to medium scale screening approach, we adapted the SCAD explant system into 96-well plate (Falcon) formats, with each well containing one biopsy. The novel 96-well SCAD pipeline was then combined with the 1280 approved small molecules from the Prestwick chemical library. Plate and liquid handling were performed using a high-throughput screening platform system composed of a Sciclone

G3 Liquid Handler from PerkinElmer (Waltham, MA, USA). On Day 0 tissues were treated either with the respective compound (1 mM stock solution) dissolved in 100 % dimethyl sulfoxide (DMSO, Carl Roth) or DMSO alone; 0.5 µl of compounds/ DMSO were transferred with a 96-array head to 200 µl DMEM/F12 medium per well to keep the final DMSO concentrations at 2.5 µM. Tissues were then incubated (37 °C; 5 % CO<sub>2</sub>) for 72 h prior to a second round of compound treatment, exchanging the cell culture medium per well and transferring 2.5 µM of compounds/ DMSO into the fresh medium. After an incubation time of another 48 h (37 °C; 5 % CO<sub>2</sub>) the tissues were harvested and fixed for histological processing and imaging.

#### **2.4 Ex vivo fascia and dermis culture— suspension assay**

The connective tissue between the panniculus carnosus and the skeleton muscle of mouse dorsal skin is part of the fascia tissue that wraps the entire body. Aiming to investigate the roles of dermis and fascia played in scarring, we established an ex vivo suspension assay. Firstly, P4 to P6 C57BL/6J neonates were sacrificed by decapitation. Then dorsal back skin with the fascia layer was carefully dissected to make 4 mm full thickness biopsies. A stereo brightfield microscope was used to separate fascia tissue from the back skin. After removing fascia tissue, the panniculus carnosus was exposed and removed to retain only dermis part. Both dermis and fascia samples were then maintained in 600 µl DMEM/F12 medium (Life Technologies) supplemented with 10 % FBS (Life Technologies), 1 % non-essential amino acid (Thermo Fisher), 1 % Glutamax (Thermo Fisher) and 1 % penicillin and streptomycin (Thermo Fisher) in a 24-well plate (Falcon) and cultured in a 37 °C incubator. After 6 days' culture the tissues were harvested and fixed for histological processing and imaging.

#### **2.5 Ex vivo fascia three-dimensional (3D) culture— fascia invasion assay**

To create a 3D environment that mimics the physiological environments *in vivo*, we established a fascia Matrigel (Corning) system. Fascia tissues were isolated by the same approach as described in chapter 2.4, but with P4 to P6 neonates of *En1*<sup>cre</sup>; R26<sup>mTmG</sup> mouse lines. Cre positive neonates from this double transgenic mouse line were detected by green fluorescent signal in dorsal skin with a Leica M205 FA stereo microscope. Matrigel was prepared by diluting the stock aliquots with plain

DMEM/F12 medium to a concentration of 6 mg/ml. Then 150 µl prepared gel was added in the center of a 35 mm cell culture dish (Ibidi). Four millimetre biopsies were made from the dorsal skin and fascia tissues were then isolated from the dorsal skin tissues. Isolated fascia tissues were then embedded into the gel and were allowed to be solidified for one hour at 37 °C. Then the tissue-gel system was maintained in DMEM/F12 medium (Life Technologies) supplemented with 10 % FBS (Life Technologies), 1 % non-essential amino acid (Thermo Fisher), 1 % Glutamax (Thermo Fisher), 1 % penicillin and streptomycin (Thermo Fisher) in a 37 °C incubator supplied with 95 % O<sub>2</sub> and 5 % CO<sub>2</sub>. Medium was changed every other day until day 4 when tissues were collected and fixed. For fixation with Matrigel system, tissues were fixed in 2 % paraformaldehyde (VWR) with 0.1 % glutaraldehyde (Sigma) for 1 hour and then washed three times with phosphate buffered saline (PBS, Life Technologies) and stored in PBS at 4 °C.

### **2.6 Invasion index and contraction index measurement**

Fascia tissues were recorded everyday by a brightfield microscope to check the invasion and contraction state of the tissues. The invasion index was calculated with the following formula:

$$\text{Invasion index} = (S_{D4} - S_{D0})/S_{D0}$$

S<sub>D4</sub> and S<sub>D0</sub> represent tissue size (including the migrated area) on Day 4 and Day 0, respectively. The contraction index was calculated with the following formula:

$$\text{Contraction index} = (T_{D0} - T_{D4})/T_{D0}$$

T<sub>D4</sub> and T<sub>D0</sub> represent original tissue size (excluding the migrated area) on Day 4 and Day 0 respectively.

### **2.7 Histology**

Except otherwise stated, all the samples were fixed overnight in 2 % paraformaldehyde (VWR) in PBS at 4 °C and washed three times with PBS. Samples were then embedded in optimal cutting temperature compound (OCT, Sakura Finetek) and snap frozen on dry ice. 6 µm frozen sections were made by a cryostat (Cryostar NX70, Thermo fisher) and frozen section slides were stored at -20 °C. Masson's

trichrome staining was applied using a trichrome stain kit (Sigma-Aldrich) according to the manufacturer's instructions. Briefly, frozen section slides were immersed in preheated Bouin's Solution at 56 °C for 15 minutes, then washed in running tap water to remove excess Bouin's reagent from the sections. Afterwards staining was performed in working Weigert's Iron Haematoxylin solution (prepared by mixing equal volume of Solution A and Solution B purchased from Sigma) for 5 minutes followed by washing in running tap water for another 5 minutes. Afterwards, slides were rinsed in deionized water and stained in Biebrich Scarlet-Acid Fuchsinn for 5 minutes. After rinsing in deionized water again, slides were placed in working phosphotungstic/phosphomolybdic acid solution for 5 minutes. Working phosphotungstic/phosphomolybdic acid solution was prepared by mixing phosphotungstic, phosphomolybdic acid and deionized water in a 1:1:2 ratio. Counterstaining was performed in aniline blue solution for 10 minutes and then in 1 % acetic acid for 2 minutes. Finally, slides were rinsed in Histol Clear (Carl Roth) and mounted with permanent mounting medium (Carl Roth). Images were recorded by a ZEISS AxioImager. Z2m (Carl Zeiss) with brightfield channel. In Masson's trichrome staining, muscle fibres and keratin are stained as red colour, collagen is stained as blue, cytoplasm is stained as light red and cell nuclei is stained as black.

## 2.8 Cell culture

Human dermal fibroblast cell line FF95 [110] was used to test the morphological changes and ECM deposition of different treatments. Forty thousand cells per well were seeded in an 8-well removable chamber slide (Ibidi) coated with 2 % gelatin (Sigma). Cells were maintained in DMEM medium supplemented with 10 % FBS (Life Technologies), 1 % non-essential amino acid (Thermo Fisher), 1 % Glutamax (Thermo Fisher), 1 % penicillin and streptomycin (Thermo Fisher) in a 37 °C incubator supplied with 95 % O<sub>2</sub> and 5 % CO<sub>2</sub>. Culture medium was changed every other day. On day 4 cells were harvested, fixed in 4 % paraformaldehyde (VWR) and washed with PBS (Life Technologies) for three times. Fixed cells can be stored at 4 °C or be processed for immunocytochemistry.

## 2.9 Immunohistochemistry

Frozen sections were equilibrated at room temperature for 10 minutes and then post-fixed for 5 min in -20 °C acetone. Sections were then rinsed three times with PBST (PBS supplemented with 0.5 % Tween-20 (Sigma)) and blocked with 10 % donkey serum or goat serum (the serum used is of the same species as the secondary antibody, Sigma). After blocking, primary antibodies diluted in PBST were added to the slide and incubated overnight at 4 °C or two hours at room temperature. Sections were then rinsed three times again with PBST and incubated with secondary antibodies for one hour at room temperature. At last, sections were washed three times with PBST to remove the excessive antibodies and mounted with fluorescent mounting medium containing 4,6-diamidino-2-phenylindole (DAPI, Thermo Fisher Scientific). Imaging was performed by an inverted Zeiss LSM 710 confocal microscope. Primary and secondary antibodies used are listed in Table 2.

Table 2. Antibodies used in immunohistochemistry

Antibody	Species	Dilution	Company	Catalog No.
Collagen I	Rabbit	1: 200	Tebu-Bio	600-401-103
Fibronectin	Rabbit	1: 200	Abcam	ab23750
CD26	Goat	1: 250	R&D Systems	AF954
CK14	Rabbit	1: 1000	Abcam	ab181595
Donkey anti rabbit AF647	Donkey	1: 500	Life Technologies	A-31573
Donkey anti goat AF647	Donkey	1: 500	Life Technologies	A-21447

## 2.10 Immunocytochemistry

The staining process of immunohistochemistry was the same as described in Immunohistochemistry (Chapter 2.9). Samples were imaged by an inverted Zeiss LSM 710 confocal microscope. Primary and secondary antibodies applied were listed in Table 3.

Table 3. Antibodies used in immunocytochemistry

Antibody	Species	Dilution	Company	Catalog No.
AF 647- Phalloidin	-	1: 500	LIFE Technologies	A22287
Tubulin	Rat	1:1000	Abcam	ab6160
Collagen I	Rabbit	1:400	Tebu-Bio	600-401-103
Collagen III	Rabbit	1:400	Abcam	ab7778
Fibronectin	Rabbit	1:400	Abcam	ab23750
Donkey anti rabbit AF647	Donkey	1: 1000	Life Technologies	A-31573
Goat anti rat AF 568	Goat	1: 1000	Life Technologies	A-11077

### 2.11 3D staining and whole mount imaging

In order to characterize the properties of fascia samples cultured in Matrigel, we fixed the whole gel (with fascia tissue embedded inside) and conducted 3D staining. Samples were immersed overnight in PBSGT (1x PBS implemented with 0.2 % gelatin (Sigma), 0.5 % Triton X-100 (Sigma) and 0.01 % thimerosal (Sigma)) at room temperature and incubated with primary antibodies diluted in PBSGT for three days at room temperature. The tissues were then washed three times with PBSGT for at least 30 min each time and incubated with secondary antibodies diluted in PBSGT for one day. Finally, tissues were rinsed three times with PBSGT and stored in PBS at 4 °C until imaging. 3D whole mount imaging was conducted with a Leica SP8 multi-photon microscope. Primary and secondary antibodies applied in 3D staining were listed in Table 4.

Table 4. Antibodies used in 3D staining

Antibody	Species	Dilution	Company	Catalog No.
αSMA	Goat	1:500	Abcam	ab21027
FAK	Rabbit	1:500	Elabscience	E-AB-33910
Ki 67	Rabbit	1:350	Abcam	ab16667
Cleaved Caspase-3	Rabbit	1:400	Cell signalling	9661S
Gli1	Rabbit	1:400	Abcam	ab49314
Donkey anti rabbit AF647	Donkey	1: 1000	Life Technologies	A-31573
Donkey anti goat AF647	Donkey	1: 1000	Life Technologies	A-21447

## 2.12 Live imaging

Fascia tissue cultured in Matrigel was fixed in 2 % low-melting agarose (Biozym) and left at room temperature to be solidified. DMEM/F12 medium without phenol red was then added to keep the tissues alive during imaging. Four-dimension (4D) time-lapse images were performed by a Zeiss AxioObserver Z1 microscope for tissues obtained from *En1<sup>cre</sup>; R26<sup>mCherry</sup>* mouse line or a Leica SP8 multi-photon microscope for tissues obtained from *En1<sup>cre</sup>; R26<sup>mTmG</sup>* mouse line. Samples were placed in a qualified incubator with heating and gas control (Ibidi). The incubator temperature was adjusted to 35 °C and was supported with 5 % CO<sub>2</sub> during imaging. Brightfield and mCherry signals were recorded for tissues from *En1<sup>cre</sup>; R26<sup>mCherry</sup>*; green fluorescent protein (GFP) and tdTomato signals were recorded for tissues from *En1<sup>cre</sup>; R26<sup>mTmG</sup>*.

## 2.13 Cell tracking

4D time-lapsed imaging was subjected to maximum intensity projection in Imaris 9.3.1 (Bitplane) or Zeiss (Blue edition) software. The projected data sets were proceeded to cell migration and cell-tracking analysis using the automatic tracking function of Imaris 9.3.1. Variables, such as spot diameter and threshold were adjusted to suit the nature of the data and the samples. For the fourth dimension of the tracks, colour ramp was applied to the individual tracks as a function of time (blue, first time point of the track; orange, last time point of the track).

## 2.14 Data analysis

3D images and time series videos were processed with Imaris 9.3.1 (Bitplane). Brightness and contrast were modified to exclude false positive signals and to obtain better visibility. Fractal analysis was conducted using the ImageJ plug in ‘FracLac’29 (FracLac 2015Sep090313a9390) [111]. Fractal dimension (D<sub>F</sub>) values and Lacunarity (Lac) values were calculated using the box counting approach (slipping and tighten grids were set at default sample sizes, threshold of minimum pixel density was set as 0.40) [112].

### **2.15 Statistics and reproducibility**

Statistical analysis was performed using GraphPad Prism software (Version 7.0, GraphPad). Until otherwise stated, all results were repeated with at least three independent experiments or three biological samples with consistent results. Cell tracking in Figure 15, Figure 16, and Figure 17 were derived with two single movies. 3D staining was performed on two samples and images were recorded at three different sites of the samples.

## III. Results

### 3.1 Characterization of the SCAD assay

In order to discover novel anti-fibrotic agents and to explore scarring mechanisms, we took advantage of the SCAD assay where uniform scars developed *ex vivo*. The SCAD tissues provided clear morphologic, histologic, and *in silico* criteria to measure and compare scar severity outcomes. Brightfield whole-mount images showed that the original SCAD tissue evolved from a flat skin piece into a contracted curved column after 5 days of culture. Trichrome staining of the corresponding samples revealed that there was an increased ECM accumulation in the scarring area of Day 5 SCAD (Figure 9a). SCADs developing scars underwent skin contraction, bending the skin towards the center of the scar. To test whether the newly formed boarder had re-epithelialized, SCAD cryo-sections were stained with cytokeratin 14 (CK14). The immunohistochemical staining depicted a clearly distinguished re-epithelialization that covered the whole SCAD tissue. Re-epithelialization originated from the skin borders and helped to easily visualize and quantify the scar contours within the skin explant (Figure 9b). SCAD samples also showed clear histological characterizations including fibroblasts that concentrated at skin centers, cross-linked connective tissue lattices that bridged between skin folds (Figure 9a and Figure 9b). Immunohistochemistry of fibrillar matrix proteins revealed abundant fibronectin and little collagen I aligned within *ex situ* scars (Figure 10). CD26 staining confirmed that most of the cells that aggregated at the scar tip are pro-scarring fibroblasts (Figure 9b and Figure 10).

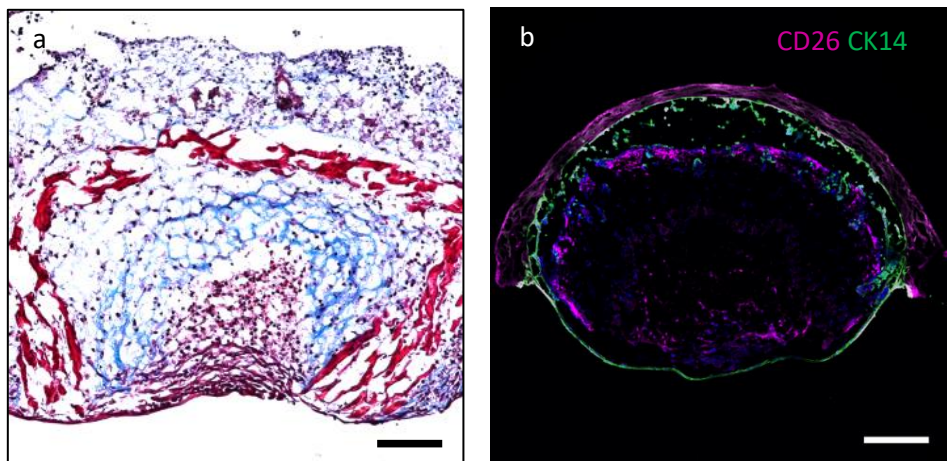


Figure 9. Histological characteristics of Day 5 SCADs. (a) Trichrome staining of the scar area in SCAD. Scarring area was encompassed by a newly formed cell layer (dark red) and inside the layer there were numerous aggregated cells (black nuclei, light red cytoplasm) and cross-linked ECM (blue). (b) Immunohistochemistry staining demonstrated that the aggregated cells were CD26 positive and the new layer that wrapped the scar was CK14 positive, implying that activated fibroblasts were gathering, and re-epithelialization occurred. Scale bar: (a), 50  $\mu$ m; (b), 100  $\mu$ m.

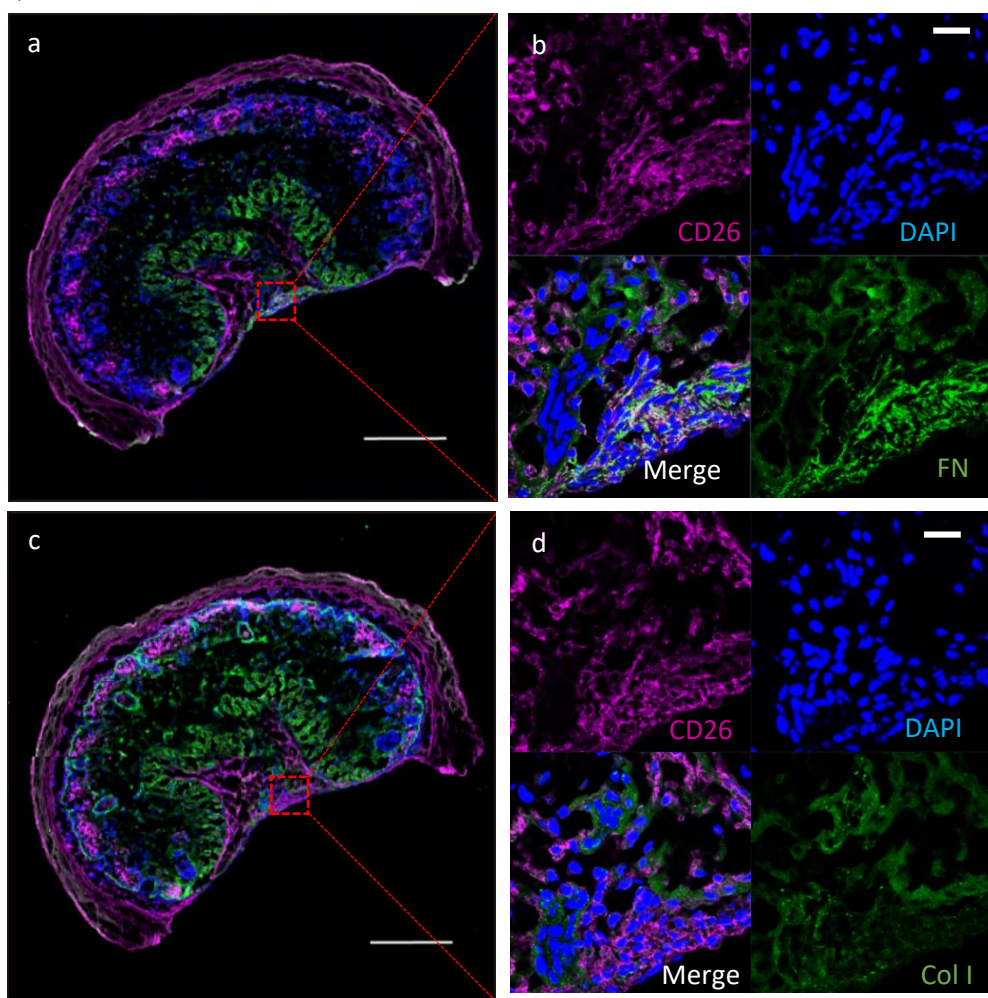


Figure 10. Immunohistochemistry staining of CD26 and ECM proteins. (a) showed CD26 and fibronectin (FN) staining in Day 5 SCAD. (c) showed CD26 and Col I staining in Day 5 SCAD. (b) and (d) showed high magnification image of scarring area in (a) and (c). Scale bar: (a) and (c), 200  $\mu$ m; (b) and (d), 20  $\mu$ m.

### 3.2 Primary screening of 1280 chemicals with the SCAD assay

Aiming to discover biological processes that underpin the fascia's wound response (fascia tissue culminated in SCAD scar), which could potentially open the door towards clinical interventional routes, we applied the whole skin SCAD assay in a high-throughput screening system (Figure 11). Our initial phenotypic screening of 1280 small molecules ( $n = 2$ , each treatment was repeated with 2 independent SCADs) identified 122 chemical hits (9.3 % hit) that were selected mainly in the light of clear differences in scar severity, showing either increased scarring or a decreased scarring or a complete absence of scars. These 120 chemicals were then manually subjected to individual chemical screening in order to further corroborate phenotypic changes ( $n = 4$ , each treatment was repeated with 2 independent SCADs). Finally, 26 top chemicals that showed consistent scarring phenotypes were selected for further evaluation. Overall, we have phenotypically screened more than 3,000 individual SCAD samples for clear histological signs of the scarring response. Some chemically treated samples showed exuberant scars that extended beyond the centre of the skin explant, some showed severe scars with strong contraction forming at closed tissue cylinders. Other chemically-treated samples that exhibited dramatically decreased scarring did not bend the tissue and the tissue itself was as flat as on Day 0 after five days' culture (Figure 12 left panel). The more severe the scars were, the stronger the contraction around the epidermal rims of the skin explant developed (Figure 12 left panel).

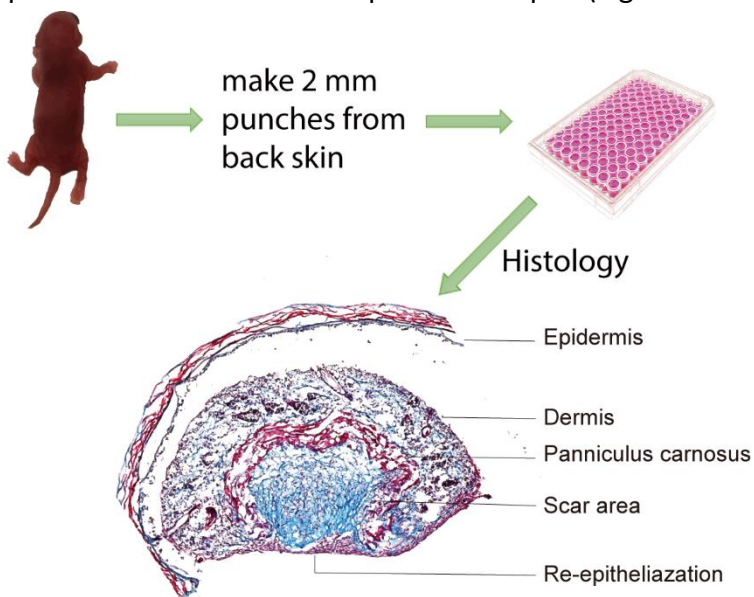


Figure 11. Scheme illustration of the screening process.

Our morphological criteria were coupled with a histological analysis of all samples ( $n=4$ ). Here, the severity of scars was further subdivided based on overall scar size, scar dimension, and extent of connective tissue formation and organization (Figure 12 middle panel). A clear range of phenotypes was observed from scarless samples marked by negligible or non-existent scars with loose and thin-linked reticular ECM to scars that emerged but had drastically different lattice organisation from normal scars, with porous and abnormally thickened ECM fibres. More severe scars also emerged with dense foci and ECM that extended beyond the borders of the original tissue. Even more severe scars exhibited dense cell foci at scar centres with ECM that overtook most of the skin explant (Figure 12 middle panel).

Next, we employed fractal analysis to further classify the severity of scars based on values of  $D_F$  and Lac of the ECM lattice organisation from individual histologic images. The  $D_F$  value reveals changes in detail with different scaling and provides a way to measure the complexity of irregular, non-Euclidean shapes. Box counting is the most popular way to measure fractal dimension. In brief, variant size ( $\varepsilon$ ) of the box is used to cover the whole object and the number of boxes ( $N$ ) needed to cover the whole object is counted.  $D_F$  is estimated as the slope of the regression line in  $\log N$  plotted against  $\log \varepsilon$ . The less the  $D_F$  value is, the less complex the tissue texture is. Lacunarity refers to the porosity of objects in morphology. The higher the value is, the more porous and heterogenous the texture is. Fractal dimension supplemented with lacunarity analysis characterized the architecture patterns of the ECM fibres with selected phenotypes in the treatments.

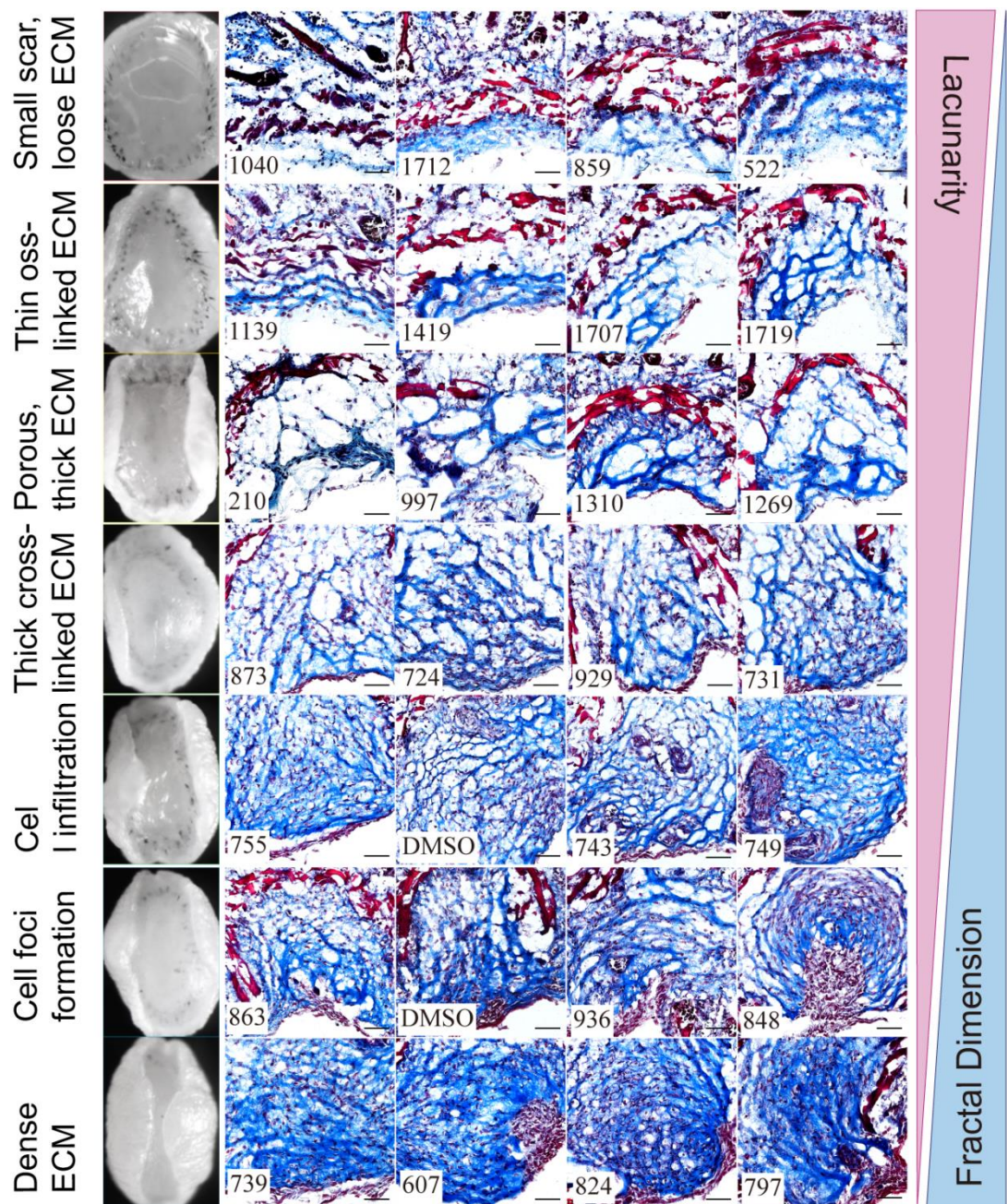


Figure 12. Brightfield phenotypes and histological analysis of the 26 selected chemicals and DMSO control. The images were ordered from top to bottom in accordance with scar severity from less scarring to exaggerated scarring. Trend of fractal dimension and lacunarity changes was shown on the right. The brightfield whole mount images are consistent with the corresponding trichrome staining images ( $n=4$ ). Scale bar, 50  $\mu$ m.

Quantification of the overall scar severity indicated that out of the 26 phenotypes, 16 samples (61.5 %) showed reduced severity of lattice organisation, whereas 10 samples (38.5 %) showed more severe scar phenotypes, compared to the control SCAD (Figure 12). From the most anti-scarring chemicals to the most pro-scarring chemicals  $D_F$  values increased and Lac values decreased, suggesting that heavy scarring is of low porosity and highly complex texture while light scarring is less complex and more porous (Figure 13). Thus, our combined SCAD/small molecule screening approach has identified a range of scar severities, all of which were classified into 26 distinct morpho-histologic phenotypes. Intriguingly, in depth analysis of the therapeutic classes of the individual compounds showed that 6 of the 16 compounds with anti-scarring response are anti-fungal or anti-bacterial, 4 are anti-inflammatory and 2 are anthelmintic. The other 4 anti-scarring compounds were antilipemic, analeptic, bronchodilatator and analgesic. In contrast the 10 pro-scarring compounds showed a variety range of treatment functions, including anti-bacterial, anti-inflammatory, bronchodilatator, antiosteoporetic and anthelmintic. Furthermore, contrastant, vasodilators, vasoconstrictors, analgesics, and antihypertensive agents were also included in this group (Table 5).

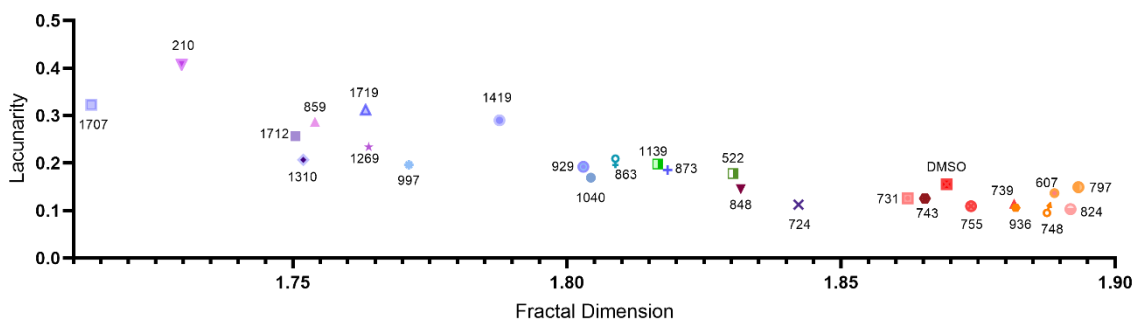


Figure 13. Fractal dimension and lacunarity analysis of 26 selected compounds from Figure 12 showed the trend that anti-scarring chemicals were of low  $D_F$  values and high Lac values, whereas pro-scarring chemicals exhibited the opposite performance of  $D_F$  values and lacunarity values, compared to the control (Ctrl) SCAD.

Table 5. Twenty-six hit chemicals screened from PCL

Nr.	Chemicals	Therapeutic class	Therapeutic effects	Mode of Action	Effect in SCAD assay*
1040	Pyrvinium pamoate	Metabolism	Anthelmintic	Casein kinase 1 $\alpha$ activator	----
1712	Flumethasone pivalate	Dermatology	Anti-inflammatory	Glucocorticoid receptor agonist	----
859	Fluvastatin sodium	Cardiovascular	Antilipemic	HMG-CoA reductase inhibitor	----
522	Thiostrepton	Infectiology	Antibacterial; Antitumor	FOXM1 inhibitor	----
1139	Itraconazole	Infectiology	Antifungal; Antitumor	Cytochrome P450 enzymes inhibitor	----
1419	Fluocinolone acetonide	Endocrinology	Anti-inflammatory	Glucocorticoid receptor agonist	----
1707	Doxapram hydrochloride	Respiratory	Analeptic	Potassium channel inhibitor	---
1719	Amorolfine hydrochloride	Infectiology	Antifungal	D-14-reductase and D-7,8-isomerase inhibitor	---
210	Fenbendazole	Infectiology	Antihelmintic	Tubulin blocker	----
997	Fluticasone propionate	Cardiovascular	Anti-inflammatory	Glucocorticoid receptor agonist	--
1310	Phenylbutazone	Metabolism	Anti-inflammatory	Prostaglandin G/H synthase 2 inhibitor	--
1269	Haloprogin	Infectiology	Antifungal		--
873	Theophylline monohydrate	Respiratory system	Bronchodilator	Adenosine receptor (antagonist)	-
724	Sulfamethoxypyridazine	Infectiology	Antibacterial	Dihydropteroate synthase inhibitor	-
929	Ketorolac tromethamine	CNS	Analgesic	Prostaglandin G/H synthase 2 inhibitor	-
731	Sulfaquinoxaline sodium salt	Infectiology	Antibacterial	Vitamin K epoxidase inhibitor	-
755	Piperacillin sodium	Infectiology	Antibacterial	Penicillin-binding proteins inhibitor	+
743	Medrysone	Metabolism	Anti-inflammatory	Glucocorticoid receptor agonist	+
749	Isoetharine mesylate salt	Respiratory	Bronchodilator	Adrenergic beta-2 agonist	+
863	Etidronate disodium	Metabolism	Antiosteoporotic	ATP inhibitor	+
936	Bephenium hydroxynaphthoate	Metabolism	Antihelmintic		+
848	Iodixanol	Diagnostic	Contrastant	X-Ray Contrast Activity	+
607	Eburnamonine (-)	CNS	Vasodilator	Muscarinic acetylcholine receptor M1-M4 modulator	+++
739	Levonordefrin	Cardiovascular	Vasoconstrictor	Adrenergic receptor alpha-2 agonist	++
797	Levomepromazine maleate	CNS	Analgesic	Adrenergic receptor & Dopamine receptor antagonist	+++
824	Benzthiazide	Cardiovascular	Antihypertensive		++ +

\* “-” represents an effect of decreasing scarring; “+” represents an effect of increasing scarring. The more symbols there are, the stronger effect the chemical showed.

### 3.3 Development of dermis and fascia explant in suspension assay

We have recently shown that the superficial fascia is a cell repository for wound myofibroblasts and scar tissue [96]. In order to characterize the effects and phenotypic responses of the chemicals to fascia directly, we zoomed in on the fascia tissue itself. We first established a whole fascia explant suspension assay in order to study the fibroblast-centric response to wounds. And we cultured the corresponding dermis tissue by the same approach. After 6 days of culture, whole fascia explants in suspension underwent a gradual process of contraction and scarring until forming an opaque and dense aggregate of scar tissue, whereas dermis tissue didn't bend itself like in the SCAD culture and displayed a whole-mount morphology as Day 0 SCAD (Figure 14). Masson's trichrome staining confirmed that dermis explants didn't curve and produced almost no ECM, whereas fascia explants formed similar ECM lattice as in the SCAD.

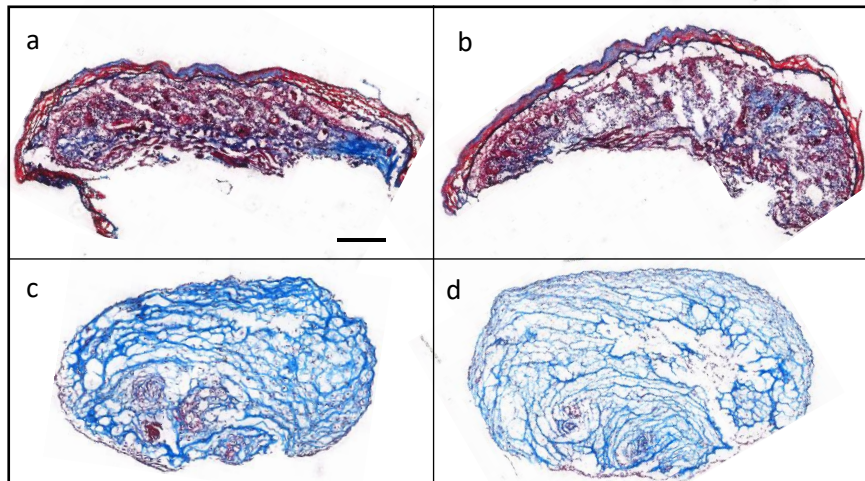


Figure 14. Trichrome staining of dermis and fascia explants cultured in suspension assay. (a) and (b) are independent samples showing that after 6 days' culture dermis tissue didn't form scarring tissue (upper panel). (c) and (d) showed two independent fascia tissues that displayed a fibrotic characteristic like scarring area in SCAD assay. Scale bar, 100  $\mu$ m.

### 3.4 Characterization of fascia invasion assay

To look more closely at the dynamics of the fibrotic cells and map the overall cell trajectory of fascia EPFs during the scarring process, we crossed our fibroblast lineage-specific promoter *Engrail1* mice to a nuclear mCherry reporter line and imaged fascia explants from the offspring. We obtained fascia explants from back skin of *En1<sup>cre</sup>; R26<sup>mCherry</sup>* and embedded tissue samples in Matrigel to form a 3D environment. *En1*-positive cells were labelled as mCherry positive cells. In order to understand the mechanism underlying the dynamic changes of fascia migration, we took live imaging of three different time points. We noticed that cells stayed still on the day the tissue was embedded in gel. After one day's equilibrium, cells adapted themselves to the surrounding microenvironment and became activated, as they began to move around inside the tissue or escaped from the original tissue (Video 1, Figure 15). Live imaging recorded that cells irregularly migrated in all directions at early stage of culture, namely from D1 to D2. After one cell run away from the living tissue, they either went forward alone or made connections with other cells to assist them in emigration, forming sprouts from the original tissue. Cell tracking also demonstrated the random movement of activated EPF at early migration stage (Figure 15 c).

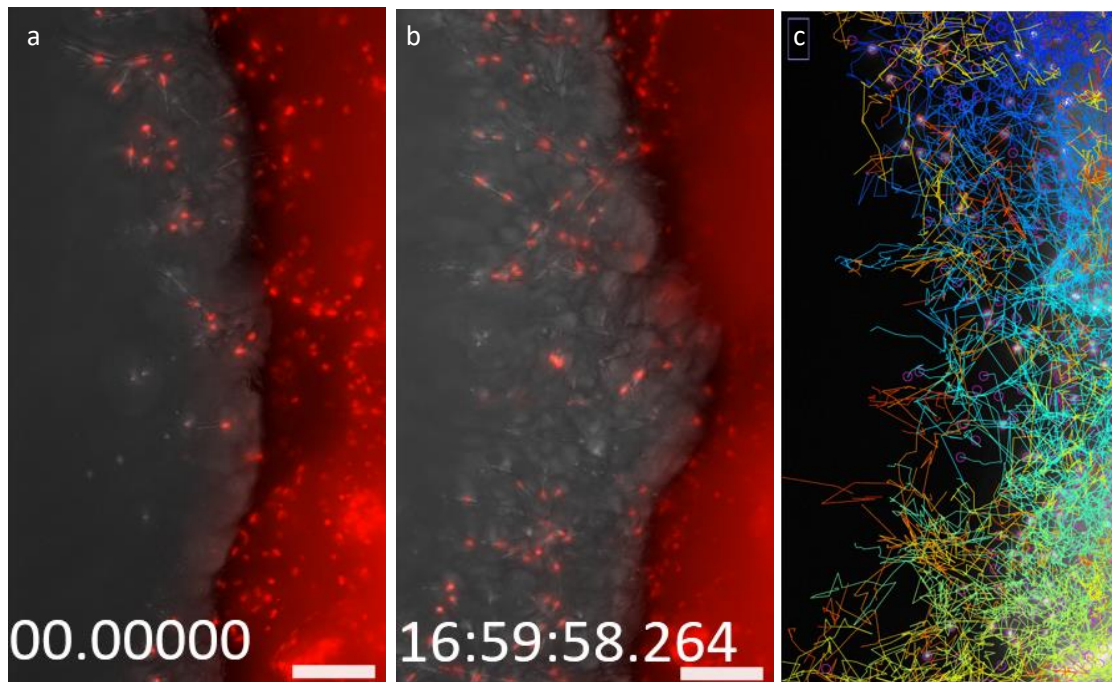


Figure 15. Snapshots and cell tracking of a live imaging recording migration of *En1<sup>cre</sup>; R26<sup>mCherry</sup>* fascia explant from D1 to D2. (a) and (b) showed starting point and end point of video. (c) showed automatic tracking of cell migration

routines, each line is a migrating trajectory for one single cell that developed from blue to orange chronologically. Scale bar, 100  $\mu$ m.

From D2 to D5 an increased number of EPFs were observed migrating out the boundary of original tissue. These activated cells showed continuous forward and backward movement (Video 2). They sprouted outside the tissue, sensed the surrounding milieu, and contacted the nearby cells by elongating cell body and producing protrusions. Finally, they found their companions when the protrusion of two cells touched each other. And then more and more cells were connected forming a network that enveloped the initial tissue. Cells within this envelop continued to move, and finally aggregated and formed cell clusters (Figure 16). This kind of movement produced a constricting power that contracted the whole tissue.

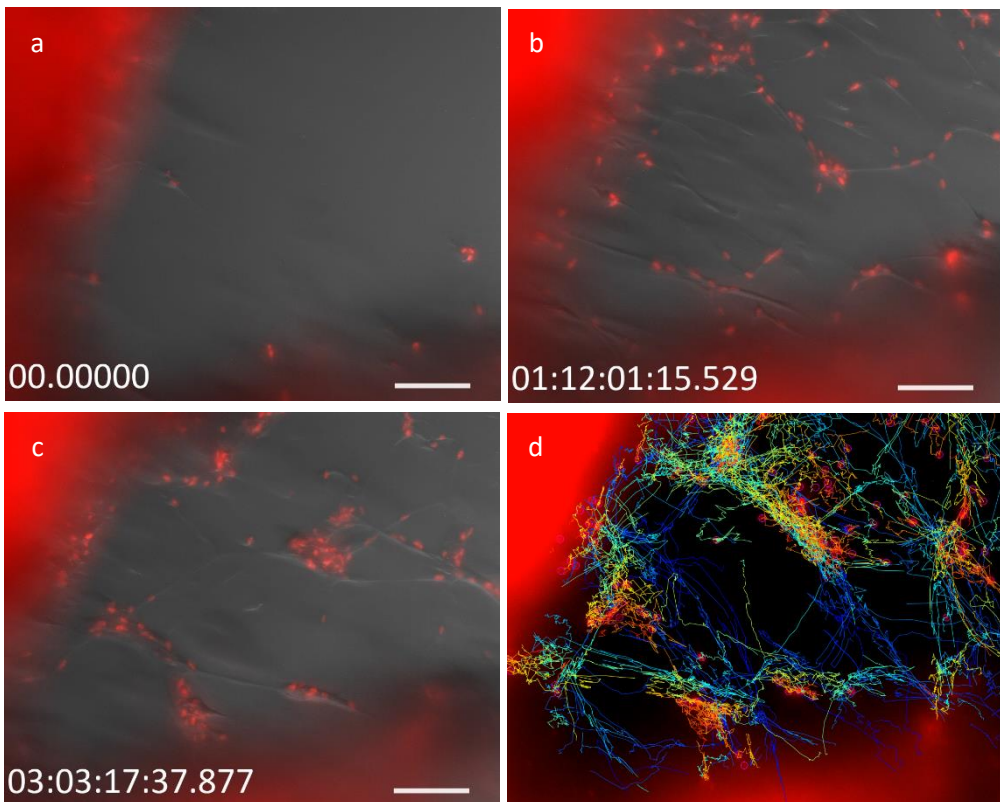


Figure 16. Snapshots of a live imaging recording migration of *En1<sup>cre</sup>; R26<sup>mCherry</sup>* fascia explant from D2 to D5. (a) showed the starting point of the video when not many cells migrated outside the tissue. (b) showed the middle point of the video when more cells escaped from the tissue and formed a network. (c) showed the end point of the video when cell clusters formed at last. Dashed lines depicted the boundary of the original tissue. (d) showed automatic tracking of cell migration routines, each line is a migrating trajectory for one single cell that developed from blue to orange chronologically. Scale bar, 100  $\mu$ m.

This tissue self-contraction was further confirmed by the contractile behavior of a small cluster of cells escaped from the initial tissue. The escaped cells were arranged

like a horizontal “L” at the beginning, but cells in the clusters continued to stretch their protrusions to sense the neighbouring environment. At last, two cells at separate ends communicated successfully and connected to each other. The size of the original tissue simultaneously slowly narrowed down along with the cell-to-cell connection (Video 3, Figure 17a and 17b). Analysis of the cell migrating trajectories by cell tracking showed that all the cells were heading to the center of the cluster, which supported the observation of self-contraction (Figure 17c).

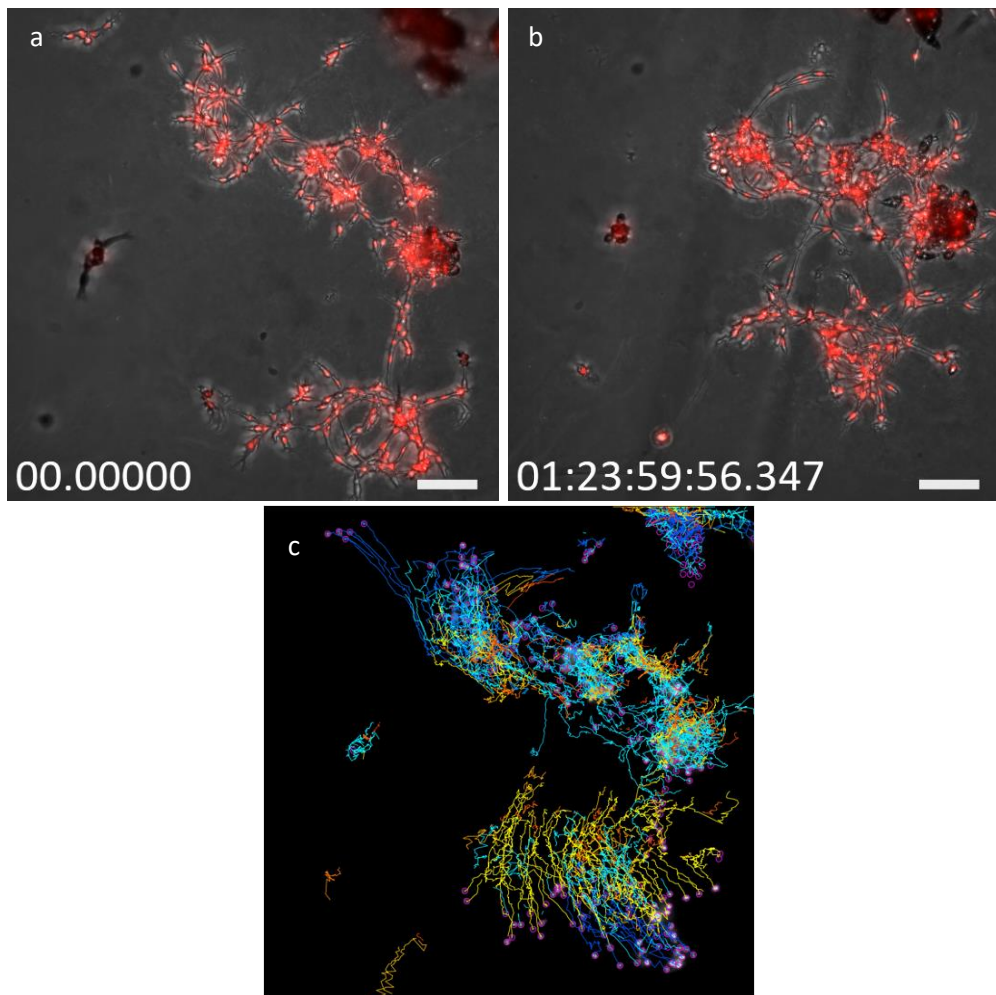


Figure 17. Snapshots of a live imaging recording migration of *En1<sup>cre</sup>; R26<sup>mCherry</sup>* fascia explant from D7 to D9. (a) showed the starting point of the video. (b) showed the end point of the video when the cell clusters contracted. (c) showed automatic tracking of cell migration routines. Each line is a migrating trajectory for one single cell that developed from blue to orange chronologically. Scale bar, 100  $\mu$ m.

In order to investigate in high detail how cell-to-cell connection occurs during migration, we took several live imaging videos using fascia tissues from *En1<sup>cre</sup>; R26<sup>mTmG</sup>* double transgenic mice, in which *En1*-positive fibroblastic lineage cells were identified as GFP positive. We found that the EPFs possessed a flexible morphology during

migration. The cells were equipped with many protrusions which facilitated them to alternate their shape for migration. These protrusions not only functioned as pseudopodium, but also acted as sensors to detect the surrounding environment (Video 4). Once the protrusion detected a protrusion from another cell, the two cells advanced towards each other and formed cell-to-cell connection (Figure 18). The countless fibroblasts were then interconnected into a web and contacted the original tissue with cells lined outwards the original borders of the tissue, showing reticulating behavior reminiscent of endothelial cells (Video 4).

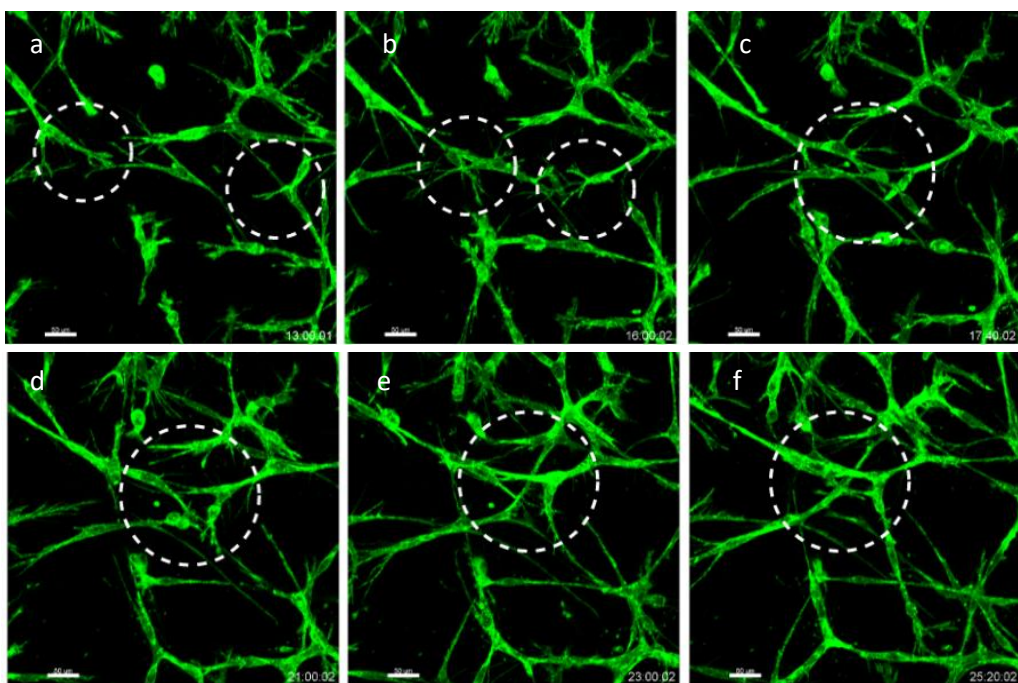


Figure 18. Chronological snapshots from a live imaging recording migration of *En1<sup>cre</sup>*; *R26<sup>mTmG</sup>* fascia explant recording EPF making connections with nearby cells (a, b, c, d, e, f). Scale bar, 50  $\mu$ m.

Tracking the tissue size and how aggressive EPFs invaded the surrounding gel every day, we found that the invasion speed accelerated from day 2 onwards (Figure 19a, Figure 20). In addition, the original size of the tissue became smaller and smaller, meaning that the tissue continued contracting (Figure 19b). Cell clustering formation was further confirmed by a live imaging recording cell migration of *En1<sup>cre</sup>*; *R26<sup>mTmG</sup>* fascia explant (Video 5). Fluorescent signal analysis of the first screenshot and the last one of video 5 showed that after 48 hours, there were some sites that showed much stronger signal than start point, suggesting that in these areas there were cell clustering formation during cell migration (Figure 21).

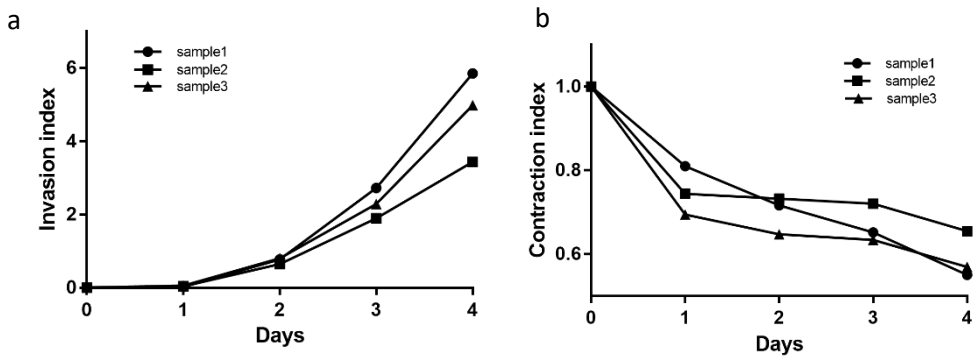


Figure 19. Dynamic changes of invasion index (a) and contraction index (b) of fascia explant in Matrigel.

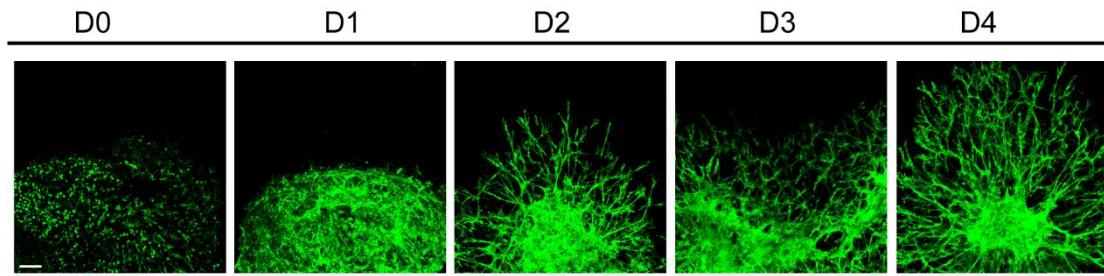


Figure 20. *En1<sup>cre</sup>; R26<sup>mTmG</sup>* fascia explant cultured in 3D Matrigel from D0 to D4. Scale bar, 100 μm.

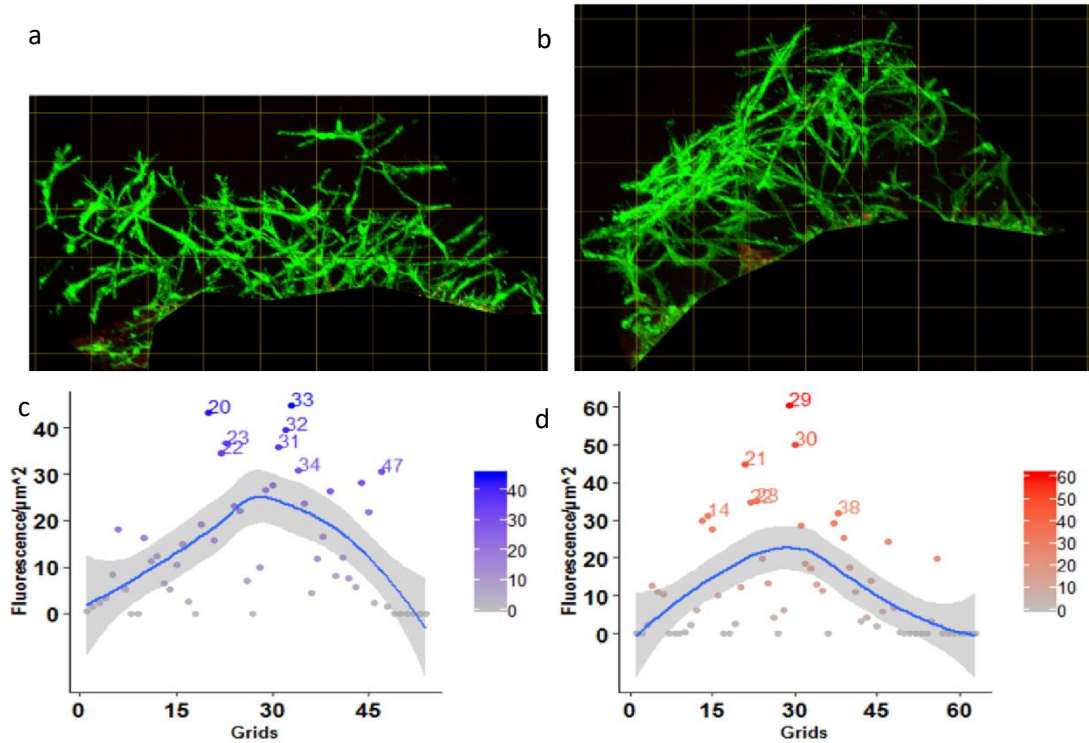


Figure 21. Clustering analysis of EPF migration. (a) and (b) showed snapshots of start point and end point from a live imaging recording EPFs migration of *En1<sup>cre</sup>; R26<sup>mTmG</sup>* fascia explant from D2 to D5. (c) and (d) compared fluorescence signal from individual grids at the two time points. Higher fluorescence means more cells at one site. The stronger fluorescence at some sites than other areas showed that EPFs formed stronger cell clustering during the migration.

The proliferation marker ki67 staining showed that cells stayed silent during the first two days and began to proliferate on Day 2 and afterwards continued proliferating until Day 4 when samples were collected. Both escaped cells and cells trapped in the original tissue kept proliferating (Figure 22).

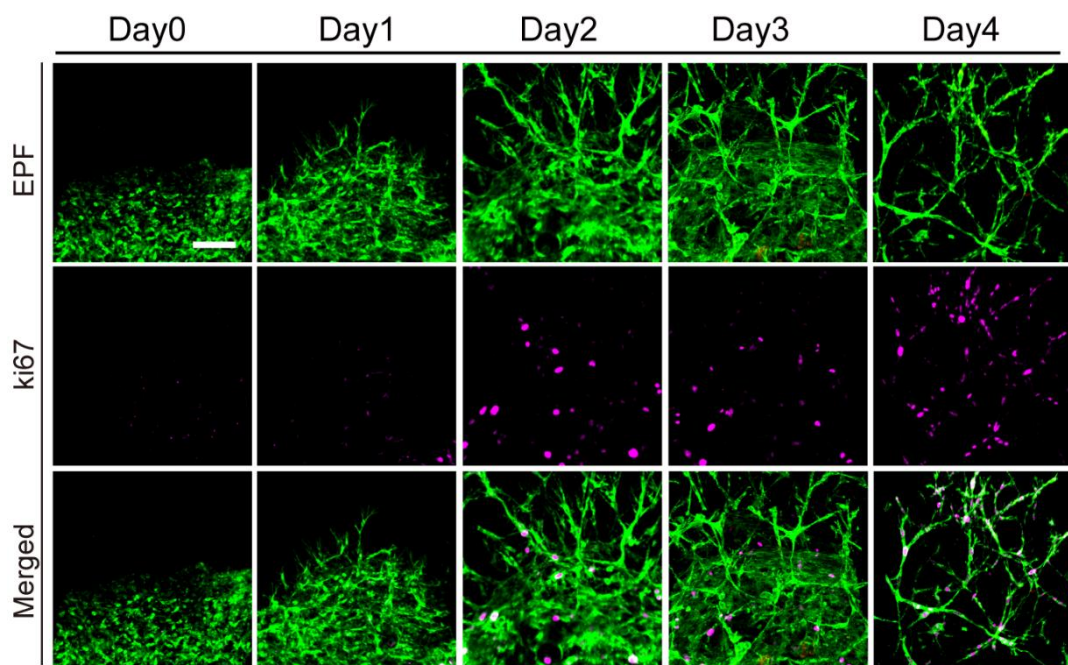


Figure 22. Ki67 staining of *En1<sup>cre</sup>; R26<sup>mTmG</sup>* fascia explants from D0 to D4. Scale bar, 100  $\mu$ m.

### 3.5 Secondary screening- retest chemical hits in fascia invasion assay

The fascia invasion assay permitted an unparalleled view of the effect of small molecules on the scarring process. Having discovered classes of chemicals with anti- and pro-scarring responses, we therefore re-tested the 26 chemicals in the fascia invasion assay. Calculation of the invasion index demonstrated that the responses of these compounds to fascia tissue were consistent with those in SCAD assays (Figure 23). Chemicals that displayed an anti-scarring activity showed a weakened migration and invasion ability, while those with pro-scarring effects provoked a more aggressive invasion capacity than DMSO control (Figure 23). By imaging treated tissues at single cell level we found that the types and numbers of protrusions produced by EPFs were proportional to their invasion ability. In the DMSO control samples, EPFs possessed a morphology of elongated spindle shape with long, thick, and bifurcated protrusions. In pro-scarring samples, EPFs not only retained long protrusions, but also with more bifurcations in protrusions, which was speculated to increase their invasion ability.

However, cell morphology of EPFs changed significantly in anti-scarring samples. EPFs in these samples didn't retain stretched thick protrusions but displayed a damaged ability to generate normal protrusions. For example, cells in itraconazole (1139) treated samples showed round shaped with just one single protrusion (Figure 24). We suspect that the thick and stretched type of protrusion may be related to the migration ability of the cell.

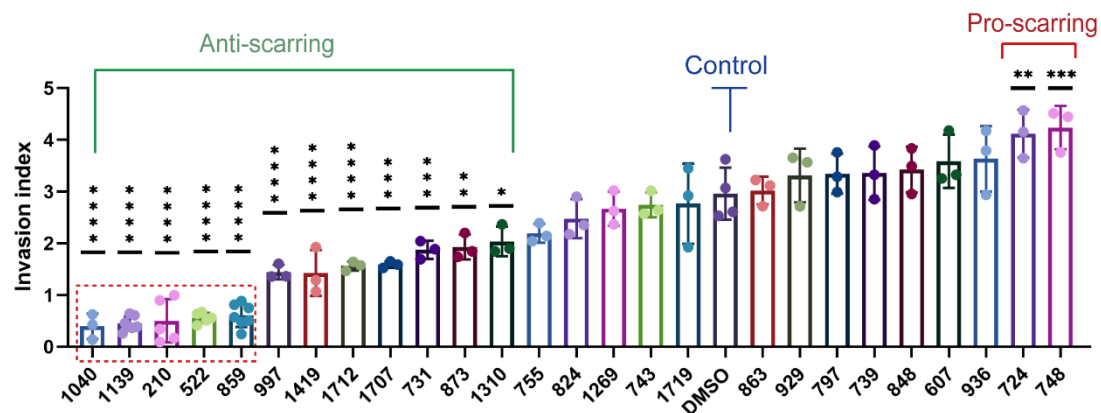


Figure 23. Invasion index of 26 hit chemicals. Red dashed line indicated the invasion level of DMSO control samples.

From the invasion index analysis combined with the morphological changes of EPF at single cell level, we chose three top chemicals to further study the mechanism of their anti-scarring effects- itraconazole (1139), Fenbendazole (210) and fluvastatin sodium salt (859) (fluvastatin is abbreviated for fluvastatin sodium salt afterwards). However, since there was massive cell death after treatment with Fenbendazole, we studied only the other two chemicals. Compared to the DMSO control, itraconazole and fluvastatin significantly perturbed the connectivity, organization of fascia EPFs and the collective migration (Figure 25a). Looking more detailed into the cell-to-cell connection we found that with itraconazole treatment cells were mostly individually distributed after migration from the original tissue. There was almost no connection between migrated cells and the original tissue and also few connections among migrated cells. With fluvastatin treatment, the connection between EPFs and tissue was not destroyed but damaged to some extent. Migrated cells still connected with their nearby counterparts, but the invasion ability was inhibited. High-magnification images showed that EPFs in fluvastatin treated fascia tissue EPFs possessed curved but not stretched protrusions, which may be the reason of the impaired invasion ability (Figure 25b).

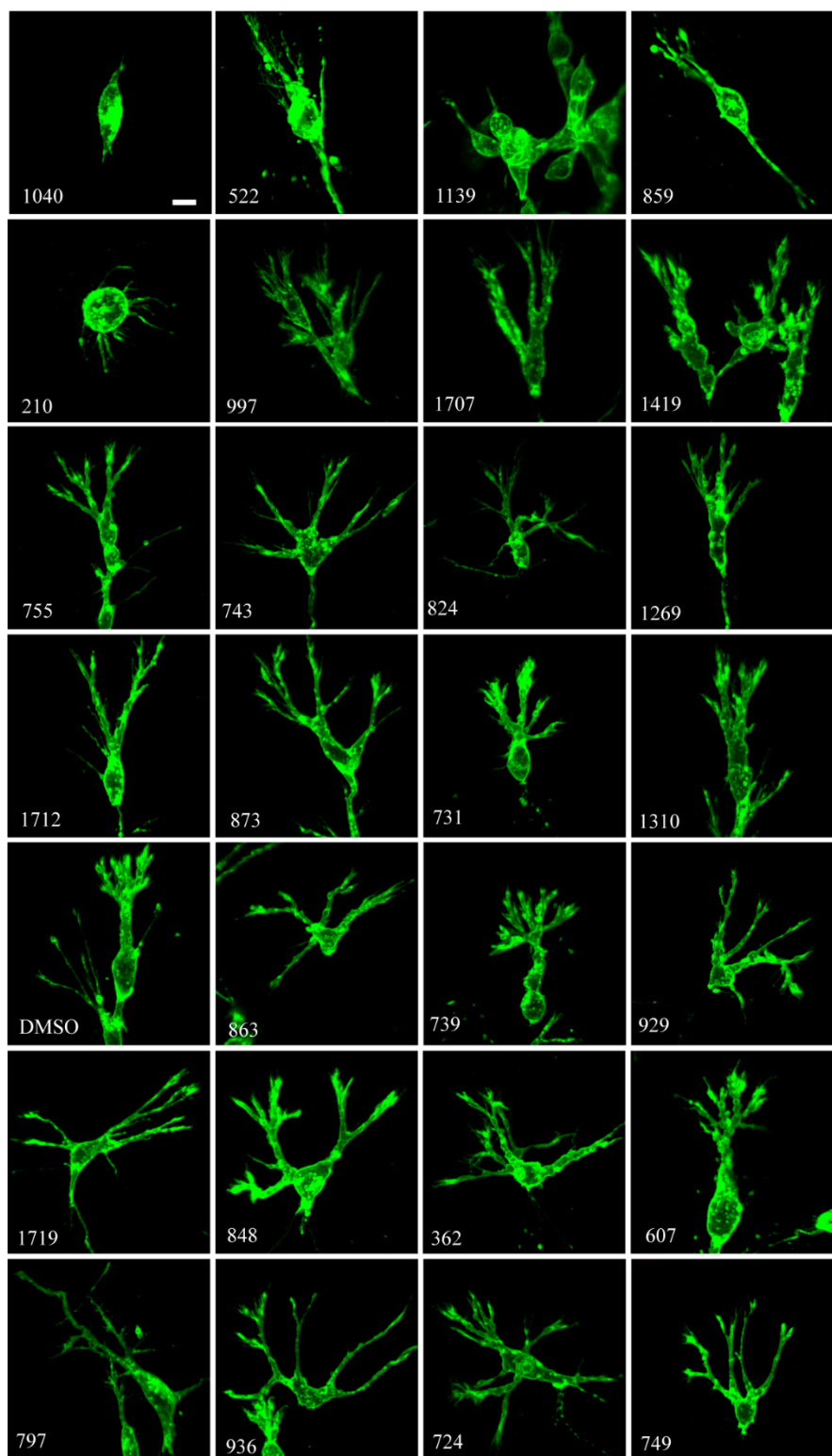


Figure 24. Morphological changes of EPFs with treatments of 26 chemicals and DMSO control at single cell level.  
Scale bar, 10  $\mu\text{m}$  ( $n = 3$ ).

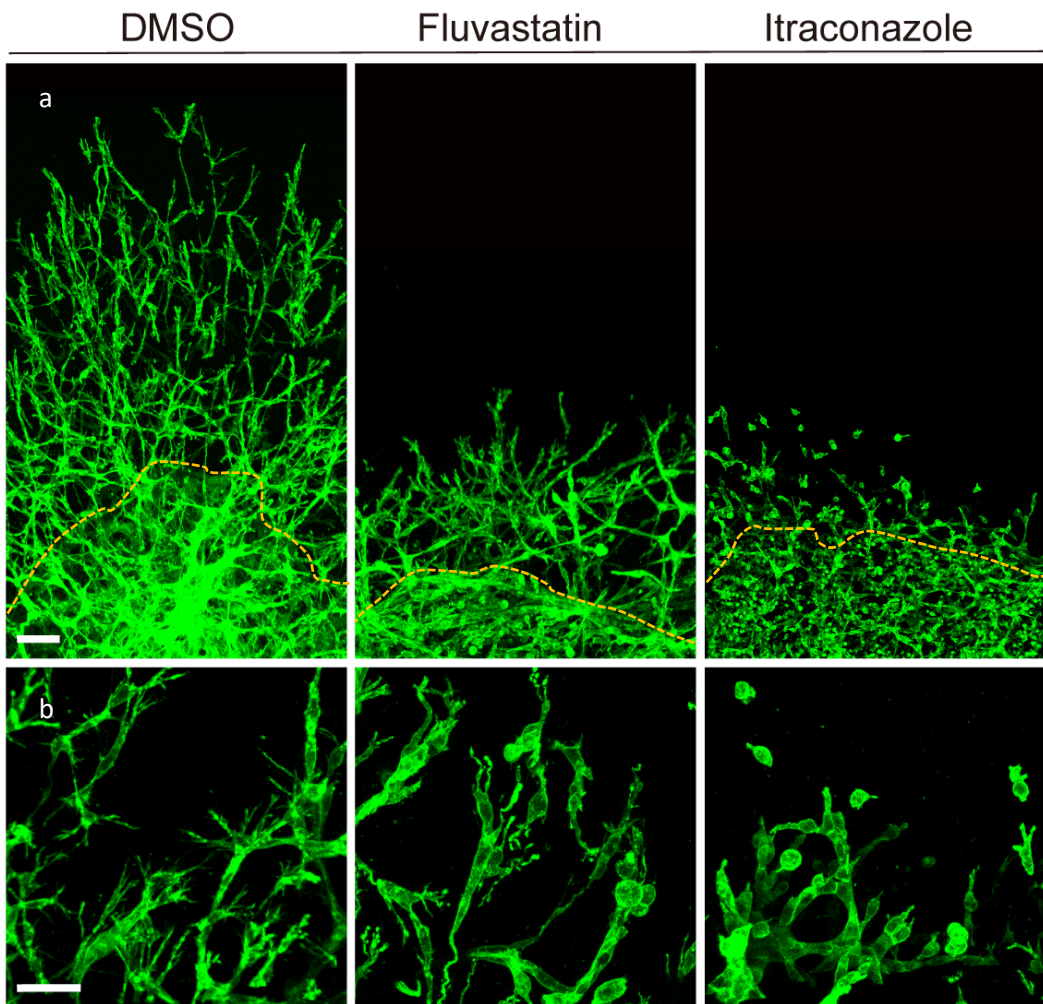


Figure 25. Multiphoton images of *En1<sup>cre</sup>; R26<sup>mTmG</sup>* fascia explant treated with DMSO, fluvastatin and itraconazole. (a) showed how far EPFs migrated outside the tissue. (b) showed morphological changes of corresponding treatment with higher magnification. Scale bar: (a), 100  $\mu$ m; (b), 50  $\mu$ m.

### 3.6 Focal adhesion kinase (FAK) is unrelated to the inhibition of fascia migration

FAK pathway is an important pathway in a diverse array of metastasis processes, such as cell adhesion, migration, and cell invasion [113]. As a key component in the FAK pathway, FAK protein has been previously reported to be required for the adhesion and migration of various cell types. Inhibition of FAK by small molecular, 1,2,4,5-Benzenetetramine tetrahydrochloride (Y15), dramatically decreased the migration of vascular endothelial cells and human hepatoblastoma cells in a dose-dependent way [114]. FAK also mediates fibroblast migration and blocking FAK activation resulted in decreased migration ability of lung fibroblasts after bleomycin treatment [115]. However, immunohistochemistry staining of FAK in our fascia samples showed that there was no difference of FAK expression among DMSO control, itraconazole and

fluvastatin treatments (Figure 26). In order to further investigate whether the FAK pathway was involved in the inhibition of fascia migration, we tested the expression of paxillin in treated samples and DMSO control. Paxillin is another important focal adhesion protein in the FAK downstream pathway and has been proven to be indispensable for directional migration of fibroblasts [116]. However, 3D staining of paxillin demonstrated no significant changes of expression in both itraconazole and fluvastatin treated tissues and the DMSO control group (Figure 27). These results suggested that FAK pathway may not be involved in the inhibition of fascia fibroblast migration by itraconazole and fluvastatin.

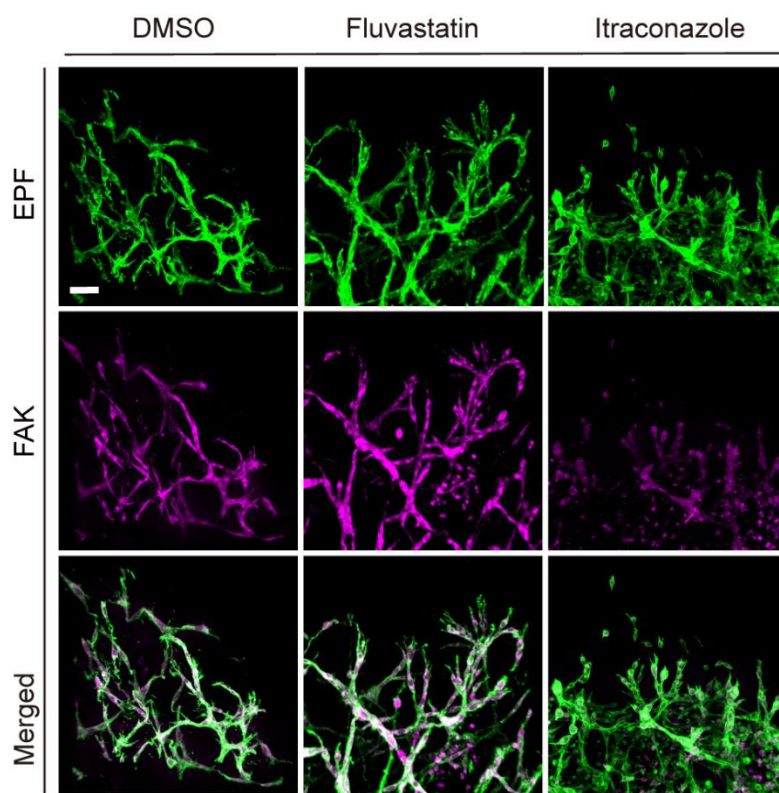


Figure 26. Immunohistochemistry staining of FAK in *En1<sup>cre</sup>; R26<sup>mTmG</sup>* fascia explants treated with DMSO, fluvastatin and itraconazole. Scale bar, 50  $\mu$ m.

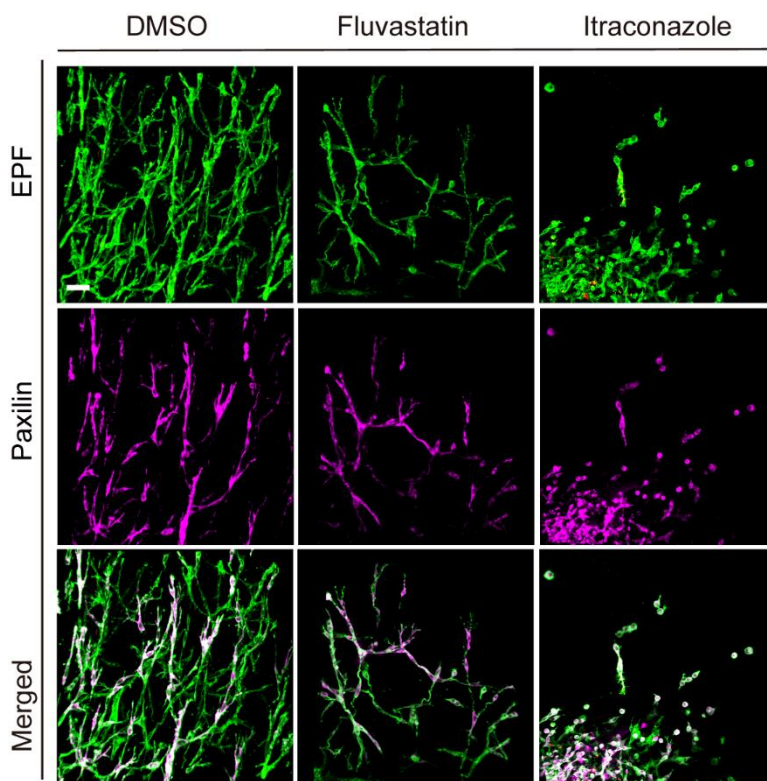


Figure 27. Immunohistochemistry staining of paxillin in *En1<sup>cre</sup>; R26<sup>mTmG</sup>* fascia explants treated with DMSO, fluvastatin and itraconazole. Scale bar, 50 µm.

### 3.7 Microtubule organization is related to the inhibition of fascia cell migration

Inspired by the morphological changes of EPFs, we detected alterations of microtubule and filamentous actin (F-actin) orientation caused by treatment of DMSO, fluvastatin and itraconazole in the FF95 fibroblast cell line. Immunostaining of tubulin and phalloidin showed that addition of DMSO resulted in a spindle-shaped, elongated fibroblast morphology, whereas fluvastatin treatment led to more elongated cell shape and itraconazole treatment resulted in polygonal, spread appearance (Figure 28). The results were consistent with the single cell images from *En1<sup>cre</sup>; R26<sup>mTmG</sup>* fascia, indicating that the alterations in morphological structure were involved in the inhibitory effect of EPF migration induced by itraconazole and fluvastatin.

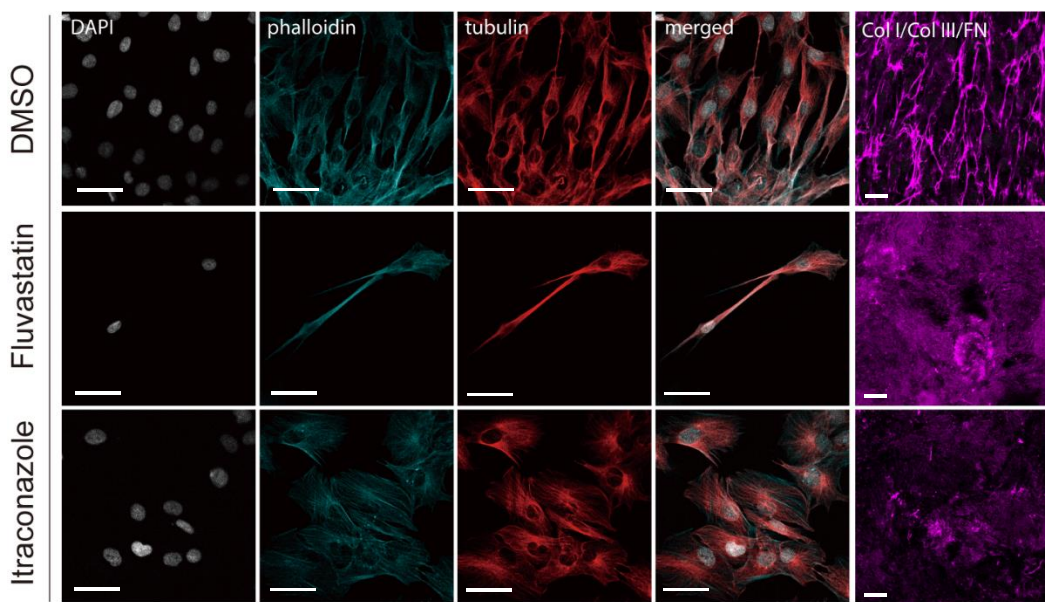


Figure 28. Immunocytochemistry staining of phalloidin, tubulin and ECM (Col I, Col III, Fibronectin) in FF95 cells treated with DMSO, fluvastatin, itraconazole. Scale bar, 50  $\mu$ m.

### 3.8 Hedgehog pathway is involved in the inhibition of fascia cell migration

The hedgehog pathway is an important signalling pathway in embryonic development and dysregulation of the pathway may lead to fibrosis of several organs. Targeting the hedgehog pathway was reported to be a therapeutic strategy to inhibit fibrosis [117]. Glioma-associated oncogene homolog 1 (Gli1) is a key transcriptional factor that carries signal to nucleus and initiates expression of target genes in hedgehog pathway [118]. Overexpression of Gli1 protein has been found in various kinds of carcinomas including glioblastomas, osteosarcoma as well as basal cell carcinoma in skin [119-121]. Here we found that itraconazole and fluvastatin performed their anti-scarring functions via the hedgehog pathway by decreasing Gli1 protein expression (Figure 29).

Itraconazole is a broad-spectrum anti-fungal drug used in adults. It has been approved for medical use in 1992 and is one of the most widely used medicine in basic health system. Recently several clinical studies have reported anti-neoplastic functions of itraconazole, including in the treatment of acute lymphoblastic leukaemia, refractory ovarian cancer, pancreatic and biliary tract cancer [122- 124]. Further investigation of the anti-cancer effect indicated that the hedgehog pathway was involved in the anti-tumour effect. It has been proven that itraconazole inhibited the hedgehog pathway by directly acting on Smoothened (SMO), a key element of the pathway that is located

in the cell membrane. Specifically, itraconazole prohibits SMO to move from cell membrane to primary cilium and thus prevents suppressor of fused protein (Sufu) to release Gli activator to the cell nucleus and finally inhibiting the pathway [125]. Immunohistochemical staining of Gli1 showed that there was only a low level of Gli1 expression in itraconazole treated samples (Figure 29). Besides, EPFs were not activated into myofibroblasts as  $\alpha$ SMA expression was trapped in the nucleus but not in cytoplasm (Figure 30). The suppression of  $\alpha$ SMA expression in itraconazole treated fascia agreed with the previous study that itraconazole can inhibit myofibroblast differentiation [126].

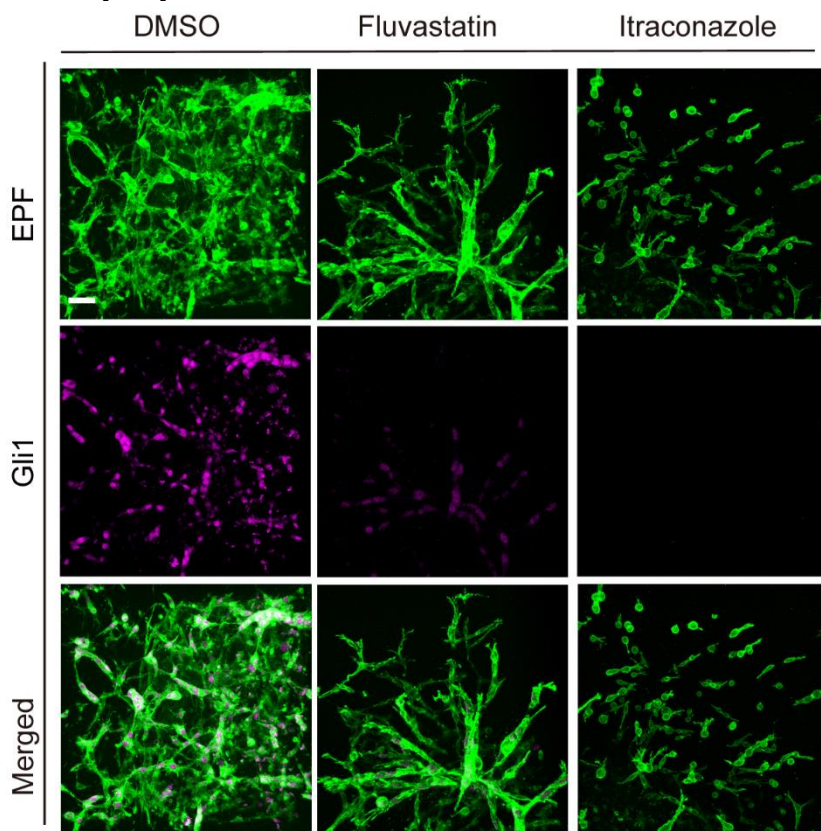


Figure 29. Gli1 staining of *En1<sup>cre</sup>; R26<sup>mTmG</sup>* fascia explants treated with DMSO and drug treatment implied that fluvastatin and itraconazole inhibited the hedgehog pathway by decreasing the expression level of Gli1. Scale bar, 50  $\mu$ m.

Fluvastatin is an inhibitor of 3-hydroxy-3-methylglutaryl-coenzyme A (HMG-CoA) reductase, which is a rate-limiting enzyme in cholesterol synthesis. It has been reported that cholesterol directly binds to SMO and activates the hedgehog pathway [127, 128]. The migrating repression effect of fluvastatin may function through inhibiting SMO activation. Immunohistochemistry in fluvastatin-treated samples demonstrated weakly expressed Gli1 protein in EPFs (Figure 29). However, intact cell-

to-cell connection and network formation still occurred, which may be because the cholesterol synthesis was not totally blocked. In addition, EPFs in fluvastatin-treated fascia samples can still be activated into myofibroblast, as expression of  $\alpha$ SMA was similar between DMSO control and fluvastatin sample, which explained the remaining cell-to-cell connection of escaped cells with fluvastatin treatment (Figure 30).

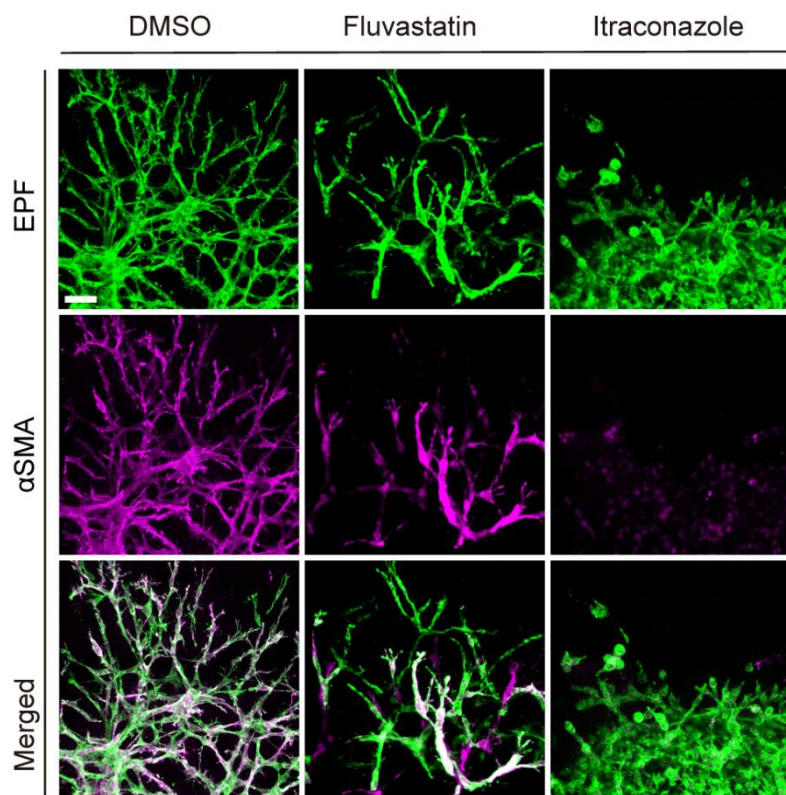


Figure 30.  $\alpha$ SMA staining of *En1<sup>cre</sup>; R26<sup>mTmG</sup>* fascia explants treated with DMSO and drug treatment implied that itraconazole inhibited myofibroblast differentiation whereas fluvastatin had no effect in myofibroblast differentiation. Scale bar, 50  $\mu$ m.

The hedgehog pathway was also reported to induce proliferation and to depress apoptosis. Ki67 and caspase 3 staining showed that cell proliferation activity of both itraconazole and fluvastatin treated samples decreased (Figure 31), whereas cell death increased (Figure 32). In addition, ECM expression was decreased by both itraconazole and fluvastatin treatments when examined in FF95 fibroblasts (Figure 28).

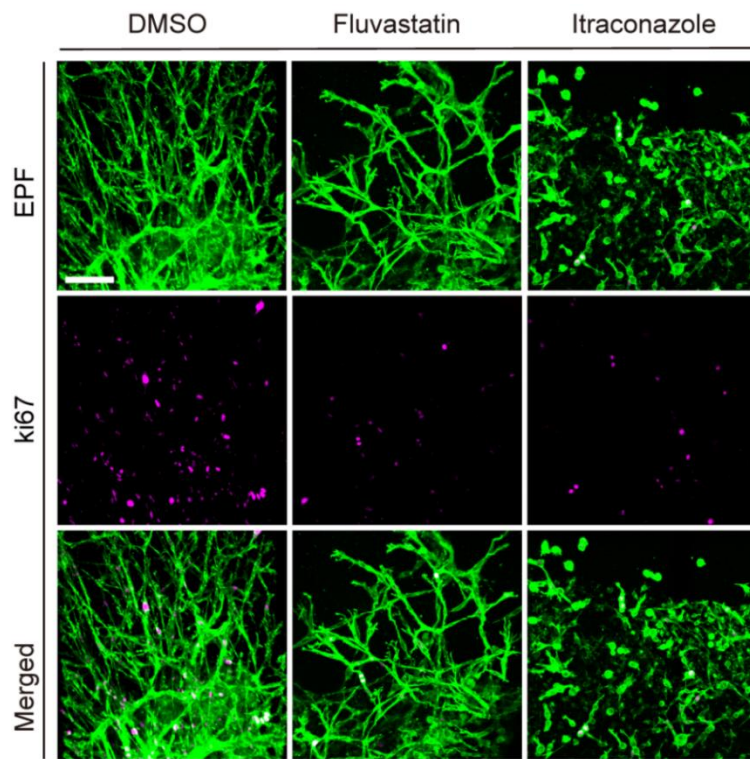


Figure 31. Ki67 staining of *En1<sup>cre</sup>; R26<sup>mTmG</sup>* fascia explants treated with DMSO, fluvastatin and itraconazole suggested an inhibitory effect in cell proliferation by fluvastatin and itraconazole treatments. Scale bar, 100  $\mu$ m.

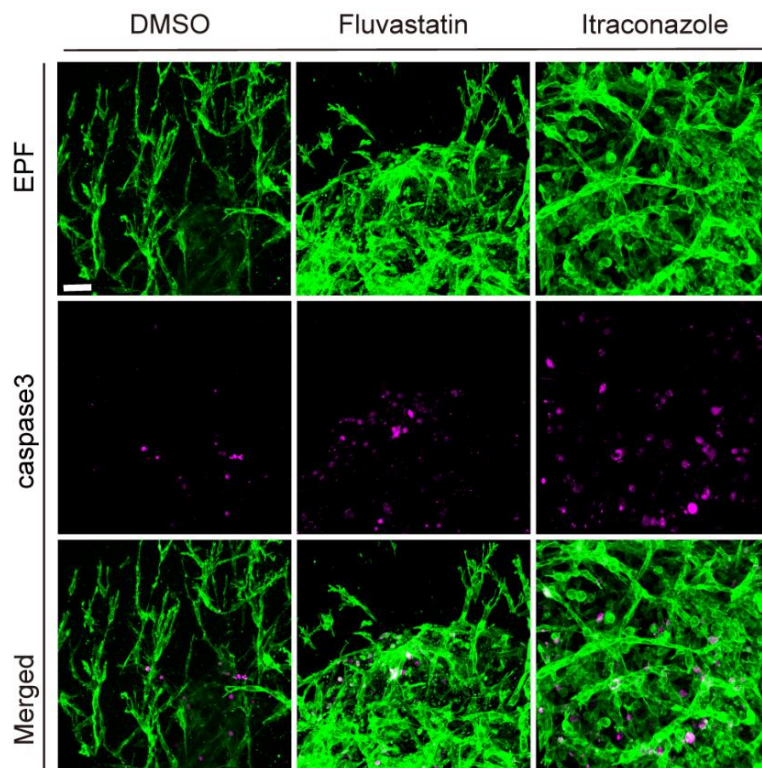


Figure 32. Caspase3 staining of *En1<sup>cre</sup>; R26<sup>mTmG</sup>* fascia explants treated with DMSO, fluvastatin and itraconazole suggested a promoting effect in cell death by fluvastatin and itraconazole treatments. Scale bar, 50  $\mu$ m.

## IV. Discussion

### 4.1 3D culture in Matrigel

As a replacement for animal experiments, standard 2D cell culture has been a widely used tool in modern biology that promoted our knowledge in fundamental biology, disease pathology, drug reaction and so on [129]. However, the monolayer cell culture on a rigid glass or plastic container can't represent the natural 3D morphology of cells due to the absence of a proper physiological microenvironment [130]. These limitations have led to growing efforts to develop 3D culture models. Compared to 2D cell culture, 3D culture systems provide scaffolds that mimic the natural *in vivo* conditions for cells to attach. Thus, the cells exhibit growth properties more similar to those found under physiological conditions. Among the various 3D scaffolds available in the market, Matrigel is the most widely utilised [131, 132]. Matrigel is a gelatinous protein mixture extracted from murine Engelbreth-Holm-Swarm (EHS) sarcoma cells. It is composed of rich matrix proteins including laminin, collagen IV, Nidogen/entactin and heparan sulphate glycoprotein, as well as a variety of growth factors [133]. Matrigel has been applied in various *ex vivo* assays such as tube formation assay, cell invasion assay and 3D spheroid culture [131].

It has been reported that many cell types would develop into a tissue-specific architecture when cultured under 3D conditions with basement membrane matrix [131, 134]. A well-known example is the tube formation assay that mimics the angiogenesis process *in vivo*. When placed in Matrigel, endothelial cells will migrate towards each other forming branching structures and finally generate tubes and lumens [135, 136]. Another example is the invasion assay to investigate the invasive capabilities of tumour cells [137, 138]. To our surprise, fascia explants cultured in Matrigel displayed not only characteristics of sprouting and branching resembling endothelial cells but also invasion ability resembling tumour cells. Live imaging that recorded neonatal fascia explant from *En1<sup>cre</sup>; R26<sup>mTmG</sup>* double transgenic mice showed EPFs migrating outside the original tissue and invading the Matrigel. Besides, escaped EPFs on the one side dragged neighbouring cells outside the tissue, on the other side extended the cell body by producing protrusions. These protrusions detected the

surroundings in search for their equivalents. Once protrusions from nearby cells contacted, the two cells were connected and then more cells interacted forming a capillary-like structure. Finally, a big network with numerous cell clusters was constructed, enveloping the whole tissue. In addition, the formation of a cell network structure outside fascia tissue simultaneously generated a contractile force that tightened the tissue itself, which has not been observed in the tube formation assay.

Invasiveness that is featured by cancer cells to enhance metastasis is another property of fascia fibroblast. It has been reported that when breast tumour cells MCF7S1 were co-cultured with mammary fibroblast in Matrigel, the expression of fibroblast specific protein 1 (FSP1) was increased in fibroblasts, which led to an enhanced level of MMP2 secretion and tumour cell invasion [139]. Interestingly, a study comparing the activity of the HT1080 fibrosarcoma cell line and normal skin fibroblasts showed that HT1080 cells in Matrigel possessed a strong migration and proliferation ability. The fibrosarcoma cells rapidly invaded the gel and formed capillary-like structure imitating endothelial cells, whereas normal fibroblast showed poor migration and invasion capability [140]. Here we demonstrate that fascia fibroblasts are featured with capacities of aggressive migration and tubule formation that are exhibited by tumour cells and endothelial cells. To the best of our knowledge, this is the first study that explored the characterization and dynamic alterations of fascia fibroblasts in a 3D culture system, at both tissue level and single cell level.

#### **4.2 Fluvastatin and itraconazole for the treatment of fibrosis**

Fluvastatin is a member of the statin family that functions as a competitive inhibitor of HMG-CoA reductase. HMG-CoA reductase is a rate-limiting enzyme in the mevalonate pathway to convert HMG-CoA into mevalonate [141]. The restrained generation of mevalonate subsequently decreases the production of the downstream molecules like isopentenyl pyrophosphate (IPP), geranyl pyrophosphate (GPP) and farnesyl pyrophosphate (FPP), and at last lowers the biosynthesis level of cholesterol. In this respect, statins are a widely used lipid-lowering medication in medicine, especially in the treatment of cardiovascular diseases [142]. Except for the classic cholesterol-lowering treatment, statins have also been applied to treat various skin disorders, as the skin is an important organ that deposits cholesterol. It has been

reported that daily intraperitoneal (IP) injection of 5mg/kg of Simvastatin alleviated the weakened wound healing in female diabetic mice ( $db+/db+$ ) by enhancing expression of VEGF [143]. Besides, Simvastatin can also reduce immune cell infiltration in infected wounds and improve the healing process [144]. In addition, statins have an anti-fibrotic effect in a variety of fibrosis models such as lung, heart, tenon and systemic sclerosis by moderating TGF- $\beta$  signalling pathway [145-148]. *In vitro* evidence proved that the anti-fibrosis effect of statins was attributed to the down regulation of CTGF, a pro-fibrotic growth factor that is provoked by TGF- $\beta$  [149]. TGF- $\beta$  plays a key role in tissue remodeling, and especially advance the progression towards fibrosis. The downstream regulation of TGF- $\beta$  signalling is usually moderated by Smad protein. However, gene expression assays showed that the expression of CTGF was independent of Smad protein. CTGF seemed to be a potential candidate to specifically arrests the pro-scarring effect of TGF- $\beta$  but reserves the other biological activities of TGF- $\beta$  [150]. In skin fibrosis statins also demonstrated an inhibitory effect of pathological scar formation. In a hypertrophic scar model of rabbit ear, low dose local injection (40  $\mu$ M) of Simvastatin, Lovastatin and Pravastatin dramatically reduced the scar elevation index by hampering CTGF levels [151]. In our study, we showed that fluvastatin sodium salt, a chemically synthesized statin, significantly hampered the migration and invasion ability of fascia fibroblasts. However, whether fluvastatin treatment can inhibit the expression of CTGF needs to be confirmed.

Itraconazole is a wide-spectrum anti-fungal medication to treat various infections including pulmonary aspergillosis, blastomycosis, as well as dermatophytosis [152-154]. The drug is orally applicable, well-tolerated, and can be used to treat fungal infection of any part of the body that suffers from a fungal infection [155, 156]. Except the anti-infection activity, itraconazole has recently been found to be able to exhibit many other properties. It was reported that itraconazole treatment inhibited the migration and tubule formation capability of human umbilical vein endothelial cells (HUVEC) *in vitro* [157]. A screening study identified itraconazole from 210 FDA approved drugs to be able to inhibit cell proliferation activity of HUVEC by arresting cell cycle at G1 phase and blocking VEGF/ bFGF dependent angiogenesis [158]. In addition, a clinical study showed that itraconazole can absolutely resolve pustules on

the arms of patients with palmoplantar pustulosis [159]. Another screening assay identified itraconazole out of about 80,000 small molecules as an effective inhibitor of myofibroblast differentiation, which may contribute to new therapeutic strategies to treat fibrosis-related diseases [160]. In the respect of skin fibrosis, itraconazole has been tested in clinics to treat hypertrophic scars and keloids as well. There was a great improvement after two weeks of itraconazole administration [161]. However, as itraconazole is an anti-fungal drug, the authors attributed the anti-scarring effect to the declined level of fungal infection [161].

In our study, itraconazole exhibited an anti-scarring effect in the SCAD fibrosis model and ameliorated the migration and invasion ability of fibroblasts in the fascia invasion assay. In addition, itraconazole damaged the network formation and cell clustering activity of fascia fibroblasts in the 3D environment. These results suggest that itraconazole is a potential candidate for the prevention and recovery treatment of skin scarring.

#### **4.3 Hedgehog pathway in fibrosis**

The hedgehog signalling pathway is of critical importance in embryonic development, organogenesis, and internal organ patterning [162]. In mammals there are three different hedgehog pathways due to the different binding ligands- Sonic Hedgehog (SHH), Indian Hedgehog (IHH) or Desert Hedgehog (DHH) [163]. Initiation of hedgehog pathway is performed by the binding of hedgehog ligand to the 12-pass transmembrane receptor patched protein (PTCH). Once HH ligand binds to PTCH, the 7-pass transmembrane protein SMO is activated and released which leads to SMO phosphorylation and accumulation in primary cilium [164]. Phosphorylated SMO induces a subsequent signalling cascade by releasing Gli1/2 protein from HH suppressor SuFu and kif7 [165]. In the absence of HH ligand, Gli1 protein is phosphorylated by protein kinase A (PKA), Glycogen synthase kinase 3 $\beta$  (GSK3 $\beta$ ) and Casein kinase 1 (CK1) and is processed to bind to transcriptional suppressor or to undergo ubiquitination for degradation [166]. In the presence of HH ligand, Gli1 will be differently phosphorylated and subsequently translocate to nucleus to activate the transcription process, initiating expression of pathway target genes including PTCH, Gli1 and Gli2 genes that generate positive feedback to the pathway, and Cyclin D1

gene that promotes cell proliferation, as well as CCND2 and CCNE1 genes that control the cell cycle [167, 168].

The hedgehog pathway is highly organised and conserved across species. Abnormal activation and dysregulation of HH signalling would result in organ hemostasis and cancer [169-171]. Recent studies reveal that hedgehog pathway plays an important role in multiple organ fibrogenesis and regeneration. SHH overexpression was found in human patients with idiopathic pulmonary fibrosis (IPF) and interstitial pneumonias [172, 173]. In a bleomycin model that causes acute injury in lung, injection of an SMO inhibitor IPI-926 ten days ahead of bleomycin treatment can significantly protect lung tissue from fibrosis, as implied by the fast recovery of body weight of the animals and decreased mRNA level of Col I and  $\alpha$ SMA [174]. Targeting the hedgehog pathway can also be a potential treatment for liver fibrosis. In a carbon tetrachloride ( $CCl_4$ )-induced liver fibrosis model, Gant61, a hedgehog inhibitor that is used to target at Gli1 and Gli2 proteins, alleviated the fibrotic level of liver and downregulated the expression level of SMO, Gli1 and Gli2 [175]. In addition, Gli1 overexpression is also detected in systemic sclerosis, renal fibrosis, and biliary fibrosis [176-178]. However, very little is known about the role of hedgehog pathway in skin scarring.

Fluvastatin inhibits the rate-controlling enzyme HMG-CoA reductase in the mevalonate pathway and leads to inhibition of cholesterol secretion. Cholesterol is the endogenous activator of SMO in the hedgehog pathway and can directly bind to SMO to activate it. The hedgehog pathway has been reported to be regulated by controlling the access of SMO to cholesterol in vertebrate [179-181]. In our study, fluvastatin treated fascia cells exhibited an atypical cell morphology that weakened the migration and invasion ability of fascia fibroblasts. By detecting Gli1 expression, we suspected that fluvastatin inhibited fascia migration by inhibiting the hedgehog pathway through downregulating Gli1 gene.

Itraconazole can directly bind to SMO and thus hinder its release to initiate the following signalling cascade events. Previous studies have shown that itraconazole can inhibit cancer progression and cancer cell proliferation, increase apoptosis, and block the cell cycle in various carcinomas through inhibiting the hedgehog pathway [182-184]. Besides, itraconazole was also administered in a murine peritoneal fibrosis

model to test the inhibition ability of fibrosis and the underlying mechanism. After 4 weeks of IP injection, the itraconazole treatment group significantly reduced the thickening of the peritoneal wall compared to the control group. At the same time, the expression of sonic hedgehog pathway related genes such as SMO, PTCH, SHH and Gli1 ligand were decreased in the itraconazole treatment group, suggesting that the SHH signalling pathway may be involved in peritoneal fibrosis and blockage of this pathway could be an alternative therapeutic choice to treat peritoneal fibrosis [185]. To the best of our knowledge, even though itraconazole has been applied to treat nonfungal cutaneous disease, but none of the research has focused the mechanism on Hedgehog pathway [186]. In our study we confirmed that itraconazole inhibited proliferation and migration of fascia fibroblasts, destroyed cell network, and promoted apoptosis by downregulating the hedgehog pathway through Gli1 protein.

## V. Summary

### 5.1 Twenty-six hits were screened from PCL with SCAD assay

From a chemical library containing 1280 agents, we screened 120 potential hits showing increased scarring or decreased scarring based on their phenotypic performance in SCAD assay. Then we conducted individual screening for these 120 chemicals and identified 26 top chemicals with consistent phenotypes. Quantification of the overall scar severity indicated that out of the 26 phenotypes, 16 chemicals (61.5 %) showed reduced severity of lattice organisation, and 10 chemicals (38.5 %) showed increased and more dense scarring. Fractal dimension and lacunarity analysis revealed that heavy scar tissue is of low porosity and highly complex texture while light scarring is more porous and less complicated.

### 5.2 Establishment and characterization of a 3D fascia invasion assay

Build on the fact that fascia is the main contributor of scarring, we established a 3D fascia invasion assay. Live imaging at different time points elaborated the dynamic process of cell migration and cell-to-cell connection. Fascia cells at first migrated randomly outside the original tissue, then migrated cells connected to following cells, forming sprouting and branching structure resembling endothelial cells. At last, this branching structure integrated into a big network that enfolded the whole tissue and contracted it. This is the first report showing the branching and network formation of fascia fibroblasts that may give a hint to explain the mechanism underlying fascia's contribution to deep wound and scarring.

### 5.3 Two top scarring- inhibiting drugs were identified

The 26 compounds described in 5.1 were re-tested in the fascia invasion assay. Based on the invasion index itraconazole and fluvastatin were identified as the top two anti-scarring compounds. Single-cell resolution images showed that fascia fibroblasts displayed different morphological changes after treatments. Upon itraconazole exposure, only a single short protrusion was formed by the cells, whereas with fluvastatin treatment, the protrusion showed a wave-pattern. In immunohistochemistry, there were no hints pointing to the inhibition of the FAK-

pathway, suggesting that the FAK-pathway may not play a key role in the anti-scarring effect of itraconazole and fluvastatin. In contrast, decreased expression of Gli1 in immunohistochemistry suggests that the hedgehog pathway may be involved in the scar-inhibiting effects of itraconazole and fluvastatin. This finding implied that inhibition of the hedgehog pathway might offer a therapeutic approach to treat scarring.

## VI. Zusammenfassung

### 5.1 Sechsundzwanzig Treffer wurden mit einem SCAD-Assay aus PCL gescreent

In der insgesamt 1280 Substanzen umfassenden chemischen Bibliothek konnten in einem ersten Screening 120 potenzielle Treffer ermittelt werden, die im SCAD-Assay eine phänotypisch erhöhte Narbenbildung bzw. eine verringerte Narbenbildung zeigten. In einem anschließenden individuellen Screening wurden 26 Top-Chemikalien mit konsistenten Phänotypen identifiziert. Die Quantifizierung des Gesamtschweregrads der Narben ergab, dass von den 26 Phänotypen 16 Chemikalien (61,5 %) einen verringerten Schweregrad der Narbenbildung zeigten, während 10 Chemikalien (38,5 %) eine erhöhte und dichtere Narbenbildung provozierten. Die Analyse der fraktalen Dimension und der Lakunenbildung ergab, dass stark ausgeprägtes Narbengewebe eine geringe Porosität und eine hochkomplexe Textur aufweist, während leichte Narben poröser und weniger komplex sind.

### 5.2 Erstellung und Charakterisierung eines 3D-Faszieninvasionsassays

Aufbauend auf der Tatsache, dass die Faszie sehr stark zur Narbenbildung beiträgt, haben wir einen 3D-Faszieninvasionsassay erstellt. Dieser erlaubte im Rahmen von Live-Imaging Aufnahmen den dynamischen Prozess der Zellmigration und des Aufbaus von Zell-zu-Zell Kontakten darzustellen. Die Faszienzellen zeigten zunächst eine zufällige Bewegung aus dem ursprünglichen Gewebeverband heraus und verbanden sich dann mit nachfolgenden Zellen, wobei Verzweigungen ausgebildet wurden, die Endothelzellen ähnelten. Diese Verästelungen wurden schlussendlich in ein Gesamtnetzwerk integriert, welches das gesamte Gewebe umhüllte und zu einer Gewebekonstruktion führte. Dies ist der erste Bericht, der die Verzweigung und Netzbildung von Faszien-Fibroblasten beschreibt und damit einen Hinweis auf den Beitrag der Faszien an tiefen Wunden und dem Verlauf der Narbenbildung gibt.

### 5.2 Zwei Wirkstoffe mit Narben-hemmenden Eigenschaften wurden identifiziert

Die unter 5.1 beschriebenen 26 Substanzen wurden im Faszieninvasionsassay getestet. Aufgrund ihres Invasionsindexes wurden itraconazol und fluvastatin als die beiden

Top-Substanzen identifiziert, die einer überschießenden Narbenbildung entgegenwirkten. Hochauflösende Einzelzellaufnahmen zeigten unterschiedliche morphologische Veränderungen bedingt durch die Behandlung. Unter Itraconazol Einfluss bildete sich eine einzelne, kurze Vorwölbung, wohingegen die fluvastatin Behandlung wellenartige Zellausläufer bedingt. In der Immunhistochemie konnten keine Hinweise auf die Hemmung des FAK-Pathways gefunden werden, was darauf hindeutet, dass der FAK-Pathway möglicherweise keine Schlüsselrolle bei der Anti-Narben-Wirkung von itraconazol und fluvastatin spielt. Im Gegensatz dazu weist die verminderte Expression von Gli1 in der Immunhistochemie darauf hin, dass der Hedgehog-Pathway in den Narben-hemmenden Effekt von itraconazol und fluvastatin involviert sein könnte. Dieser Befund impliziert, dass die Hemmung des Hedgehog-Pathway einen therapeutischen Ansatz liefern könnte, um eine Narbenbildung zu behandeln.

## VII. References

- [1] Gurtner GC, Werner S, Y Barrandon, Longaker MT. Wound repair and regeneration. *Nature*, 453: 314–321 (2008).
- [2] Sun BK, Siprashvili Z, Khavari PA. Advances in skin grafting and treatment of cutaneous wounds. *Science*, 346: 941–945 (2014).
- [3] Golebiewska EM, Poole AW. Platelet secretion: from haemostasis to wound healing and beyond. *Blood Rev*, 29: 153–162 (2015).
- [4] Werner S, Grose R. Regulation of wound healing by growth factors and cytokines. *Physiol Rev*, 83: 835–870 (2003).
- [5] Singer AJ, and Clark RA. Cutaneous wound healing. *N Engl J Med*, 341: 738–746 (1999).
- [6] Wilgus TA, Roy S, McDaniel JC. Neutrophils and wound repair: positive actions and negative reactions. *Adv Wound Care*, 2: 379–388 (2013).
- [7] Velnar T, Bailey T, Smrkolj V. The wound healing process: an overview of the cellular and molecular mechanisms. *J Int Med Res*, 37: 1528–1542 (2009).
- [8] Koh TJ, DiPietro LA. Inflammation and wound healing: the role of the macrophage. *Expert Rev Mol Med*, 11: 13–23 (2011).
- [9] Wynn TA, Vannella KM. Macrophages in tissue repair, regeneration, and fibrosis. *Immunity*, 44: 450–462 (2016).
- [10] Eming SA, Krieg T, Davidson JM, Inflammation in wound repair: molecular and cellular mechanisms. *J Invest Dermatol*, 127: 514–525 (2007).
- [11] Williamson D, Harding K. Wound healing. *Medicine*, 32: 4–7 (2004).
- [12] Darby IA, Hewitson TD. Hypoxia in tissue repair and fibrosis. *Cell Tissue Res*, 365: 553–562 (2016).

- [13] Greaves NS, Ashcroft KJ, Baguneid M, Bayat A. Current understanding of molecular and cellular mechanisms in fibroplasia and angiogenesis during acute wound healing. *J Dermatol Sci*, 72: 206–217 (2013).
- [14] Thittamaranahalli Muguregowda Honnegowda, Pramod Kumar, Echalasara Govindarama Padmanabha Udupa, Sudesh Kumar, Udaya Kumar, Pragna Rao. Role of angiogenesis and angiogenic factors in acute and chronic wound healing. *Plast Aesthet Res*, 2: 243–249 (2015).
- [15] Tracy LE, Minasian RA, Caterson EJ. Extracellular matrix and dermal fibroblast function in the healing wound. *Adv Wound Care (New Rochelle)*, 5: 119–136 (2016).
- [16] Midwood KS, Williams LV, Schwarzauer JE. Tissue repair and the dynamics of the extracellular matrix. *Int J Biochem Cell Biol*, 36: 1031–1037 (2004).
- [17] Darby IA, Laverdet B, Bonté F, and Desmoulière A. Fibroblasts and myofibroblasts in wound healing. *Clin Cosmet Investig Dermatol*, 7: 301–311 (2014).
- [18] Bin Li and James H-C. Wang. Fibroblasts and Myofibroblasts in Wound Healing: Force Generation and Measurement. *J Tissue Viability*, 20(4): 108–120 (2011).
- [19] Pastar I, Stojadinovic O, Yin NC, Ramirez H, Nusbaum AG, Sawaya A, Patel SB, Khalid L, Isseroff RR, Tomic-Canic M. Epithelialization in wound healing: a comprehensive review. *Adv Wound Care (New Rochelle)*, 3: 445–464 (2014).
- [20] Ito M, Liu Y, Yang Z, Nguyen J, Liang F, Morris RJ, Cotsarelis G. Stem cells in the hair follicle bulge contribute to wound repair but not to homeostasis of the epidermis. *Nat Med*, 11: 1351–1354 (2005).
- [21] Blanpain C, Fuchs E. Plasticity of epithelial stem cells in tissue regeneration. *Science*, 344: 1242281 (2014).
- [22] Donati G, Rognoni E, Hiratsuka T, Liakath Ali K, Hoste E, Kar G, Kayikci M, Russell R, Kretzschmar K, Mulder KW, Teichmann SA, Watt FM. Wounding induces dedifferentiation of epidermal Gata6 cells and acquisition of stem cell properties. *Nat Cell Biol*, 19: 603–613 (2017).

- [23] Miller SJ, Burke EM, Rader MD, Coulombe PA, Lavker RM. Re-epithelialization of porcine skin by the sweat apparatus. *J Invest Dermatol*, 110: 13–19 (1998).
- [24] Mark A. Seeger and Amy S. Paller. The Roles of Growth Factors in Keratinocyte Migration. *Adv Wound Care (New Rochelle)*, 4(4): 213–224 (2015).
- [25] Gill SE, Parks WC. Metalloproteinases and their inhibitors: regulators of wound healing. *Int J Biochem Cell Biol*, 40: 1334–1347 (2008).
- [26] Smith MM, Melrose J. Proteoglycans in normal and healing skin. *Adv Wound Care (New Rochelle)*, 4: 152–173 (2015).
- [27] Meilang Xue and Christopher J. Jackson. Extracellular Matrix Reorganization During Wound Healing and Its Impact on Abnormal Scarring. *Adv Wound Care (New Rochelle)*, 4(3): 119–136 (2015).
- [28] Zomer HD, Trentin AG. Skin wound healing in humans and mice: Challenges in translational research. *J Dermatol Sci*, 90:3-12 (2018).
- [29] Peacock Jr EE, Madden JW, Trier WC. Biologic basis for the treatment of keloids and hypertrophic scars. *South Med J*, 63: 755–760 (1970).
- [30] Mancini RE, Quaife JV. Histogenesis of experimentally produced keloids. *J Invest Dermatol*, 38: 143–181 (1962).
- [31] Bailey J, Waite A, Clayton W, Rustin M. Application of topical mito-mycin C to the base of shave-removed keloid scars to prevent their recurrence. *Br J Dermatol*, 156: 682–686 (2007).
- [32] Gauglitz GG, Korting HC, Pavicic T, Ruzicka T, and Jeschke MG. Hypertrophic scarring and keloids: pathomechanisms and current and emerging treatment strategies. *Mol Med*, 17:113–125 (2011).
- [33] Lewis WH, Sun KK. Hypertrophic scar: a genetic hypothesis. *Burns*, 16: 176–178 (1990).
- [34] Deitch EA, Wheelahan TM, Rose MP, Clothier J, Cotter J. Hypertrophic burn scars: analysis of variables. *J Trauma*, 23: 895–898 (1983).

- [35] Armour A, Scott PG, and Tredget EE. Cellular and molecular pathology of HTS: basis for treatment. *Wound Repair Regen*, 15: S6–17 (2007).
- [36] Hunasgi S, Koneru A, Vanishree M, Shamala R. Keloid: A case report and review of pathophysiology and differences between keloid and hypertrophic scars. *J Oral Maxillofac Pathol*, 17: 116–120 (2013).
- [37] Rabello FB, Souza CD, Juñior JA. Update on hypertrophic scar treatment. *Clinics*, 69: 565–573 (2014).
- [38] Lane JE, Waller JL, Davis LS. Relationship between age of ear piercing and keloid formation. *Pediatrics*, 115: 1312–1314 (2005).
- [39] Halim AS, Emami A, Salahshourifar I, Kannan TP. Keloid scarring: understanding the genetic basis, advances, and prospects. *Arch Plast Surg*, 39: 184–189 (2012).
- [40] Ogawa R. Keloid and hypertrophic scars are the result of chronic inflammation in the reticular dermis. *Int J Mol Sci*, 18: 606–615 (2017).
- [41] Kaartinen I. Treatment of hypertrophic scars and keloids. *Duodecim*, 132: 1439–1447 (2016).
- [42] Mari W, Alsabri SG, Tabal N, Younes S, Sherif A, Simman R. Novel insights on understanding of keloid scar: Article Review. *J Am Coll Clin Wound Spec*, 7: 1–7 (2015).
- [43] Chike-Obi CJ, Cole PD, Brissett AE. Keloids: pathogenesis, clinical features, and management. *Semin Plast Surg*, 23:178–184 (2009).
- [44] Karppinen SM, Heljasvaara R, Gullberg D, Tasanen K, Pihlajaniemi T. Toward understanding scarless skin wound healing and pathological scarring. *F1000 Faculty Rev*, 787–798 (2019).
- [45] Herpina A, Lelong C, Favrel P. Transforming growth factor- $\beta$ -related proteins: an ancestral and widespread superfamily of cytokines in metazoans. *Dev Comp Immunol*, 2: 461–485 (2004).
- [46] Schmid P, Itin P, Cherry G, Bi C, Cox DA. Enhanced expression of transforming growth factor-beta type I and type II receptors in wound granulation tissue and hypertrophic scar. *Am J Pathol*, 152: 485–493 (1998).

- [47] Lee TY, Chin GS, Kim WJ, Chau D, Gittes GK, Longaker MT. Expression of transforming growth factor beta 1, 2, and 3 proteins in keloids. *Ann Plast Surg*, 43: 179–184 (1999).
- [48] Xia W, Phan TT, Lim IJ, Longaker MT, Yang GP. Complex epithelial-mesenchymal interactions modulate transforming growth factor beta expression in keloid-derived cells. *Wound Repair Regen*, 12: 546–556 (2004).
- [49] Messadi DV, Le A, Berg S, Huang G, Zhuang W, Bertolami CN. Effect of TGF-beta 1 on PDGF receptors expression in human scar fibroblasts. *Front Biosci*, 3: a16–a22 (1998).
- [50] Fujiwara M, Muragaki Y, Ooshima A. Upregulation of transforming growth factor-beta1 and vascular endothelial growth factor in cultured keloid fibroblasts: relevance to angiogenic activity. *Arch Dermatol Res*, 297: 161–169 (2005).
- [51] Xuechuan Li, Yu Wang, Bo Yuan, Huizhong Yang, Liang Qiao. Status of M1 and M2 type macrophages in keloid. *Int J Clin Exp Pathol*, 10(11): 11098–11105 (2017).
- [52] Xue M, Jackson CJ. Extracellular matrix reorganization during wound healing and its impact on abnormal scarring. *Adv Wound Care (New Rochelle)*, 4: 119–136 (2015).
- [53] Friedman DW, Boyd CD, Mackenzie JW, Norton P, Olson RM, Deak SB. Regulation of collagen gene expression in keloids and hypertrophic scars. *J Surg Res*, 55: 214–222 (1993).
- [54] Al-Attar A, Mess S, Thomassen JM, Kauffman CL, Davison SP. Keloid pathogenesis and treatment. *Plastic Reconstr Surg*, 117: 286–300 (2006).
- [55] Sidgwick GP, Bayat A. Extracellular matrix molecules implicated in hypertrophic and keloid scarring. *J Eur Acad Dermatol Venereol*, 26: 141–52 (2012).
- [56] Rowlatt U. Intrauterine wound healing in a 20-week human foetus. *Virchows Arch A Pathol Anat Histol*, 381: 353–361 (1979).
- [57] Buchanan EP, Longaker MT, Lorenz HP. Fetal skin wound healing. *Adv Clin Chem*, 48: 137–161 (2009).

- [58] Mast BA, Flood LC, Haynes JH, DePalma RL, Cohen IK, Diegelmann RF, Krummel TM. Hyaluronic acid is a major component of the matrix of fetal rabbit skin and wounds: implications for healing by regeneration. *Matrix*, 11: 63–68 (1991).
- [59] Beanes SR, Hu F-Y, Soo C, Dang CMH, Urata M, Ting K, Atkinson JB, Benhaim P, Hedrick MH, Lorenz HP. Confocal microscopic analysis of scarless repair in the fetal rat: defining the transition. *Plast Reconstr Surg*, 109: 160–170 (2002).
- [60] McCallion RL, Ferguson MWJ. Fetal wound healing and the development of anti-scarring therapies for adult wound healing. In: Clark RAF, editor. *The Molecular and Cellular Biology of Wound Repair*, Plenum Press, 561–600 (1996).
- [61] Mast BA, Diegelmann RF, Krummel TM, Cohen IK. Scarless wound healing in the mammalian fetus. *Surg Gynecol Obstet*, 174: 441–451 (1992).
- [62] Carlos Zgheib, Junwang Xu, Kenneth W Liechty. Targeting Inflammatory Cytokines and Extracellular Matrix Composition to Promote Wound Regeneration. *Adv Wound Care (New Rochelle)*, 3(4): 344–355 (2014).
- [63] Whitby DJ, Ferguson MW. Immunohistochemical localization of growth factors in fetal wound healing. *Dev Biol*, 147: 207–215 (1991).
- [64] Ferguson MW, O’Kane S. Scar-free healing: from embryonic mechanisms to adult therapeutic intervention. *Philos Trans R Soc B Biol Sci*, 359: 839–850 (2004).
- [65] Sciubba JJ, Waterhouse JP, Meyer J. A fine structural comparison of the healing of incisional wounds of mucosa and skin. *J Oral Pathol*, 7: 214–227 (1978).
- [66] Hakkinen L, Uitto VJ, Larjava H. Cell biology of gingival wound healing. *Periodontol*, 24: 127–152 (2000).
- [67] Stephens P, Davies KJ, Khatee T, Shepherd JP, Thomas DW. A comparison of the ability of intra-oral and extra-oral fibroblasts to stimulate extracellular matrix reorganization in a model of wound contraction. *J Dent Res*, 75: 1358–1364 (1996).
- [68] Eslami A, Gallant-Behm CL, Hart DA, Wiebe C, Honardoust D, Gardner H, Hakkinen L, Larjava HS. Expression of integrin alphavbeta6 and TGF-beta in scarless vs scar-forming wound healing. *J Histochem Cytochem*, 57: 543–557 (2009).

- [69] Yang J, Tyler LW, Donoff RB, Song B, Torio AJ, Gallagher GT, Tsuji T, Elovic A, McBride J, Yung CM, Galli SJ, Weller PF, Wong DT. Salivary EGF regulates eosinophil-derived TGF-alpha expression in hamster oral wounds. *Am J Physiol*, 270: 191–202 (1996).
- [70] Szpaderska AM, DiPietro LA. Inflammation in surgical wound healing: friend or foe? *Surgery*, 137: 571–575 (2005).
- [71] Chen L, Arbieva ZH, Guo S, Marucha PT, Mustoe TA, DiPietro LA. Positional differences in the wound transcriptome of skin and oral mucosa. *BMC genomics*, 11: 471–485 (2010).
- [72] Seifert AW, Kiama SG, Seifert MG, Goheen JR, Todd M. Palmer, Malcolm Maden. Skin shedding and tissue regeneration in African spiny mice (*Acomys*). *Nature*, 489: 561–565 (2012)
- [73] Santos DM, Rita AM, Casanellas I, Brito Ova A, Araújo IM, Power D, Gustavo T. Ear wound regeneration in the African spiny mouse *Acomys cahirinus*. *Regeneration (Oxf)*, 3: 52–61 (2016).
- [74] Halim AS , Emami A , Salahshourifar L, Kannan TP. Keloid scarring: understanding the genetic basis, advances, and prospects. *Arch Plast Surg*, 39: 184–189 (2012).
- [75] Driskell RR, Lichtenberger BM, Hoste E, Kretzschmar K, Simons BD, Charalambous M, Ferron SR, Herault Y, Pavlovic G, Ferguson-Smith AC, Watt FM. Distinct fibroblast lineages determine dermal architecture in skin development and repair. *Nature*, 504: 277–281 (2013).
- [76] Rinkevich Y, Walmsley GG, Hu MS, Maan ZN, Newman AM, Drukker M, Januszyk M, Krampitz GW, Gurtner GC, Lorenz HP, Weissman IL, Longaker MT. Skin fibrosis. Identification and isolation of a dermal lineage with intrinsic fibrogenic potential. *Science*, 348: aaa2151 (2015).
- [77] Correa-Gallegos D, Jiang D, Christ S, Ramesh P, Ye H, Wannemacher J, Kalgudde Gopal S, Yu Q, Aichler M, Walch A, Mirastschijski U, Volz T, Rinkevich Y. Patch repair of deep wounds by mobilized fascia. *Nature*, 576: 287–292(2019).

- [78] Bordoni B, Mahabadi N, Varacallo M. Anatomy, Fascia. [Updated 2019 Jul 30]. In: StatPearls [Internet] <https://www.ncbi.nlm.nih.gov/books/NBK493232/>
- [79] Kumka M, Bonar J. Fascia: a morphological description and classification system based on a literature review. *J Can Chiropr Assoc*, 56: 179–191 (2012).
- [80] Cowman MK, Schmidt TA, Raghavan P, Stecco A. Viscoelastic properties of hyaluronan in physiological conditions. *F1000 Res*, 4: 622–632 (2015).
- [81] Langevin HM, Nedergaard M, and Howe AK. Cellular control of connective tissue matrix tension. *J Cell Biochem*, 114: 1714–1719 (2013).
- [82] Bordoni B, Zanier E. Understanding fibroblasts in order to comprehend the osteopathic treatment of the fascia. *Evid Based Complement Alternat Med*, 860934 (2015).
- [83] Langevin HM, Bouffard NA, Fox JR, Palmer BM, Wu J, Iatridis JC, Barnes WD, Badger GJ, Howe AK. Fibroblast cytoskeletal remodeling contributes to connective tissue tension. *J Cell Physiol*, 226: 1166–1175 (2011).
- [84] Helene M. Langevin, Maiken Nedergaard, and Alan Howe. Cellular control of connective tissue matrix tension. *J Cell Biochem*, 114:8 (2013).
- [85] Hedley G. Notes on visceral adhesions as fascial pathology. *J Bodyw Mov Ther*, 14: 255–261 (2010).
- [86] Bunker T. Time for a new name for frozen shoulder— contracture of the shoulder. *Shoulder Elbow*, 1: 4–9 (2009).
- [87] Gabbiani G, Majno G. Dupuytren's contracture: fibroblast contraction? An ultrastructural study. *Am J Pathol*, 66: 131–146 (1972).
- [88] Pedrelli A, Stecco C, Day JA. Treating patellar tendinopathy with fascial manipulation. *J Bodyw Mov Ther*, 13: 73–80 (2009).
- [89] Picelli A, Ledro G, Turrina A, Stecco C, Santilli V, Smania N. Effects of myofascial technique in patients with subacute whiplash associated disorders: a pilot study. *Eur J Phys Rehabil Med*, 47: 561–568 (2011).

- [90] Stecco A, Stecco C, Macchi V, Porzionato A, Ferraro C, Masiero S, De Caro R. MRI study and clinical correlations of ankle retinacula damage and outcomes of ankle sprain. *Surg Radiol Anat*, 33: 881–890 (2011a).
- [91] Klingler W, Velders M, Hoppe K, Pedro M, Schleip R. Clinical relevance of fascial tissue and dysfunctions. *Curr Pain Headache Rep*, 18: 439–445 (2014).
- [92] Lau FH, Pomahac B. Wound healing in acutely injured fascia. *Wound Repair Regen*, 22: 14–17 (2014).
- [93] Wachtel TL, Wright TE, Kuhn MA, Ko F, Robson MC. Fascial incisions heal faster than skin: a new model of abdominal wall repair. *Surgery*, 129: 203–208 (2001).
- [94] Dubay DA, Wang X, Kirk S, Adamson B, Robson MC, Franz MG. Fascial fibroblast kinetic activity is increased during abdominal wall repair compared to dermal fibroblasts. *Wound Repair Regen*, 12: 539–545 (2004).
- [95] Ogawa R, Akaishi S, Huang C, Dohi T, Aoki M, Omori Y, Koike S, Kobe K, Akimoto M, Hyakusoku H. Clinical Applications of Basic Research that Shows Reducing Skin Tension Could Prevent and Treat Abnormal Scarring: The importance of fascial/subcutaneous tensile reduction sutures and flap surgery for keloid and hypertrophic scar. *J Nippon Med Sch*, 78: 68–76 (2011).
- [96] Ogawa R, Akita S, Akaishi S, Aramaki-Hattori N, Dohi T, Hayashi T, Kishi K, Kono T, Matsumura H, Muneuchi G, Murao N, Nagao M, Okabe K, Shimizu F, Tosa M, Tosa Y, Yamawaki S, Ansai S, Inazu N, Kamo T, Kazki R, Kuribayashi S. Diagnosis and treatment of keloids and hypertrophic scars-Japan Scar Workshop Consensus Document 2018. *Burns Trauma*, 7: 39–78 (2019).
- [97] Wong VW, Sorkin M, Glotzbach JP, Longaker MT, Gurtner GC. Surgical approaches to create murine models of human wound healing. *J Biomed Biotechnol*, 969618: 1–8 (2011).
- [98] Gerber PA, Buhren BA, Schrumpf H, Homey B, Zlotnik A, Hevezi P. The top skin-associated genes: a comparative analysis of human and mouse skin transcriptomes. *Biol Chem*, 395: 577–591 (2014).

- [99] Lindblad WJ. Considerations for selecting the correct animal model for dermal wound-healing studies. *J Biomater Sci Polym Ed*, 19: 1087–1096 (2008).
- [100] Cibelli J, Emborg ME, Prockop DJ, Roberts M, Schatten G, Rao M, Harding J, Mirochnitchenko O. Strategies for improving animal models for regenerative medicine. *Cell Stem Cell*, 12: 2–5 (2013).
- [101] Sertkaya A, Birkenbach A, Berlind A, Eyraud J. Examination of clinical trial costs and barriers for drug development. US Department of health and human services, office of the assistant secretary for planning and evaluation report. 1: 1–92 (2014).
- [102] [Internet] Drug approval process.  
<https://www.fda.gov/Drugs/DevelopmentApprovalProcess/default.htm>.
- [103] [Internet] Drug development process.  
<https://www.fda.gov/Drugs/default.htm.5>.
- [104] Ashburn TT, Thor KB. Drug repositioning: identifying and developing new uses for existing drugs. *Nat Rev Drug Discov*, 3: 673–683 (2004).
- [105] Pushpakom S, Iorio F, Evers PA, Escott KJ, Hopper S, Wells A, Doig A, Guilliams T, Latimer J, McNamee C, Norris A, Sanseau P, Cavalla D, Pirmohamed M. Drug repurposing: progress, challenges and recommendations. *Nat Rev Drug Discov*, 18: 41–58 (2019).
- [106] Swinney DC, Anthony J. How were new medicines discovered? *Nat Rev Drug Discovery*, 10: 507–519 (2011).
- [107] Yarchoan R, Brouwers P, Spitzer AR, Grafman J, Safai B, Perno CF, Larson SM, Berg G, Fischl MA, Wichman A, Thomas RV, Brunetti A, Schmidt PJ, Myers CE, Broder S. Response of human-immunodeficiency-virus-associated neurological disease to 3'-azido-3'-deoxythymidine. *Lancet*, 1: 132–135 (1987).
- [108] Osborne R. First novel anti-Tuberculosis drug in 40 years. *Nat Biotechnol*, 31: 89–91 (2013).

- [109] Jung ML, Contreras JM, Morice C, Simon JM, Didier B and Langer T. The Prestwick Chemical Library® - a valuable tool for screening. Online Poster, <http://www.prestwickchemical.com/pdf/2018-pcl-a-valuable-tool.pdf>.
- [110] Jiang D, Singh K, Muschhammer J, Schatz S, Sindrilaru A, Makrantonaki E, Qi Y, Wlaschek M, Scharffetter-Kochanek K. MSCs rescue impaired wound healing in a murine LAD1 model by adaptive responses to low TGF- $\beta$ 1 levels. *EMBO Rep*, e49115 (2020).
- [111] Karperien A. FracLac for ImageJ. 1999–2013; <http://rsb.info.nih.gov/ij/plugins/fraclac/> FLHelp/Introduction.htm
- [112] Jiang D, Correa-Gallegos D, Christ S, Stefanska A, Liu J, Ramesh P, Rajendran V, Santis MMD, Wagner DE, Rinkevich Y. Two succeeding fibroblastic lineages drive dermal development and the transition from regeneration to scarring. *Nat Cell Biol*, 20: 422–431 (2018).
- [113] Parsons JT. Focal adhesion kinase: the first ten years. *J Cell Sci*, 116: 1409–1416 (2003).
- [114] Yu H, Gao M, Ma Y, Wang L, Shen Y, Liu X. Inhibition of cell migration by focal adhesion kinase: Time-dependent difference in integrin-induced signalling between endothelial and hepatoblastoma cells. *Int J Mol Med*, 41: 2573–2588 (2018).
- [115] Zhao XK, Cheng Y, Cheng ML, Yu L, Mu M, Li H, Liu Y, Zhang B, Yao Y, Guo H, Wang R, Zhang Q. Focal adhesion kinase regulates fibroblast migration via integrin beta-1 and plays a central role in fibrosis. *Sci Rep*, 19276: 1–12 (2016).
- [116] German AE, Mammoto T, Jiang E, Ingber DE, Mammoto A. Paxillin controls endothelial cell migration and tumour angiogenesis by altering neuropilin 2 expression. *J Cell Sci*, 127: 1672–1683 (2014).
- [117] Hu L, Lin X, Lu H, Chen B and Bai Y. An overview of Hedgehog signaling in fibrosis. *Mol Pharmacol*, 87: 174–182 (2015).
- [118] Carpenter RL, Lo HW. Hedgehog pathway and GLI1 isoforms in human cancer. *Discov Med*, 13: 105–113 (2012).

- [119] Kinzler KW, Bigner SH, Bigner DD, Trent JM, Law ML, O'Brien SJ, Wong AJ, Vogelstein B. Identification of an amplified, highly expressed gene in a human glioma. *Science*, 236: 70–73 (1987).
- [120] Roberts WM, Douglass EC, Peiper SC, Houghton PJ, Look AT. Amplification of the gli gene in childhood sarcomas. *Cancer Res*, 49: 5407–5413(1989).
- [121] Dahmane N, Lee J, Robins P, Heller P, Ruiz i Altaba A. Activation of the transcription factor Gli1 and the Sonic hedgehog signaling pathway in skin tumors. *Nature*, 389: 876–881 (1997).
- [122] Vreugdenhil G, Raemaekers JM, van Dijke BJ, de Pauw BE. Itraconazole and multidrug resistance: Possible effects on remission rate and disease-free survival in acute leukemia. *Ann Hematol*, 67: 107–109 (1993).
- [123] Tsubamoto H, Sonoda T, Yamasaki M, and Inoue K. Impact of combination chemotherapy with itraconazole on survival of patients with refractory ovarian cancer. *Anticancer Res*, 34: 2481–2487 (2014).
- [124] Tsubamoto H, Sonoda T, Ikuta S, Tani S, Inoue K and Yamanaka N. Combination chemotherapy with itraconazole for treating metastatic pancreatic cancer in the second-line or additional setting. *Anticancer Res*, 35: 4191–4196 (2015).
- [125] Kim J, Tang JY, Gong R, Kim J, Lee JJ, Clemons KV, Chong CR, Chang KS, Fereshteh M, Gardner D, Reya T, Liu JO, Epstein EH, Stevens DA, Beachy PA. Itraconazole, a commonly used anti-fungal that inhibits Hedgehog pathway activity and cancer growth. *Cancer Cell*, 17: 388–399 (2010).
- [126] Bollong MJ, Yang B, Vergani N, Beyer BA, Chin EN, Zambaldo C, Wang D, Chatterjee AK, Lairson LL, Schultz PG. Small molecule-mediated inhibition of myofibroblast transdifferentiation for the treatment of fibrosis. *Proc Natl Acad Sci*, 114: 4679–4684 (2017).
- [127] Huang P, Nedelcu D, Watanabe M, Jao C, Kim Y, Liu J, Salic A. Cellular cholesterol directly activates Smoothened in Hedgehog signaling. *Cell*, 166: 1176–1187 (2016).

- [128] Luchetti G, Sircar R, Kong JH, Nachtergael S, Agner A, Byrne EFX, Covey DF, Siebold C, Rohatgi R. Cholesterol activates the G-protein coupled receptor Smoothened to promote Hedgehog signaling. *eLife*, 5: e20304 (2016).
- [129] Kapałczyńska M, Kolenda T, Przybyła W, Zajęczkowska M, Teresiak A, Filas V, Ibbs M, Bliźniak R, Łuczewski Ł, Lamperska K. 2D and 3D cell cultures – a comparison of different types of cancer cell cultures. *Arch Med Sci*, 14: 910–919 (2018).
- [130] Cukierman E, Pankov R, Yamada KM. Cell interactions with three dimensional matrices. *Curr Opin Cell Biol*, 14: 633–639 (2002).
- [131] Kleinman HK, Martin GR. Matrigel: basement membrane matrix with biological activity. *Semin Cancer Biol*, 15: 378–386 (2005).
- [132] Kleinman HK, McGarvey ML, Liotta LA, Robey PG, Tryggvason K, Martin GR. Isolation and characterization of type IV procollagen, laminin, and heparan sulphate proteoglycan from the EHS sarcoma. *Biochemistry*, 21: 6188–6193 (1982).
- [133] Bentona G, Arnaoutova I, Georgea J, Kleinman HK, Koblinskic J. Matrigel: From discovery and ECM mimicry to assays and models for cancer research. *Adv Drug Deliv Rev*, 80: 3–18 (2014).
- [134] Kleinman HK, Martin GR. Matrigel: basement membrane matrix with biological activity. *Semin Cancer Biol*, 15: 378–386 (2005).
- [135] Arnaoutova I, George J, Kleinman HK, Benton G. The endothelial cell tube formation assay on basement membrane turns 20: state of the science and the art. *Angiogenesis*, 12: 267–274 (2009).
- [136] Mettouchi A. The role of extracellular matrix in vascular branching morphogenesis. *Cell Adhes Migr*, 6: 528–534 (2012).
- [137] Albini A, Iwamoto Y, Kleinman HK, Martin GR, Aaronson SA, Kozlowski JM, McEwan RN. A rapid in vitro assay for quantitating the invasive potential of tumor cells. *Cancer Res*, 47: 3239 –3245 (1987).
- [138] Bae SN, Arand G, Azzam H, Pavasant P, Torri J, Frandsen TL, Thompson EW. Molecular and cellular analysis of basement membrane invasion by human breast

- cancer cells in Matrigel-based in vitro assays. *Breast Cancer Res Treat*, 24: 241–255 (1993).
- [139] Olsen C, Moreira J, Lukanidin EM, Ambartsumian NS. Human mammary fibroblasts stimulate invasion of breast cancer cells in a three-dimensional culture and increase stroma development in mouse xenografts. *BMC Cancer*, 10: 1–16 (2010).
- [140] Kramer RH, Bensch KG, Wong J. Invasion of reconstituted basement membrane by metastatic human tumor cells. *Cancer Res*, 46: 1980–1989 (1986).
- [141] Endo A, Kuroda M, Tsujita Y. ML-236A, ML-236B, and ML-236C, new inhibitors of cholesterologenesis produced by penicillium citrinum. *J Antibiot*, 29: 1346–1348 (1976).
- [142] Istvan ES, Deisenhofer J. Structural mechanism for statin inhibition of HMG-CoA reductase. *Science*, 292: 1160–1164 (2001).
- [143] Bitto A, Minutoli L, Altavilla D, Polito F, Fiumara T, Marini H, Galeano M, Calò M, Cascio PL, Bonaiuto M, Migliorato A, Caputi AP, Squadrato F. Simvastatin enhances VEGF production and ameliorates impaired wound healing in experimental diabetes. *Pharmacol Res*, 57: 159–169 (2008).
- [144] Rego AC, Araújo Filho I, Damasceno BP, Egito ES, Silveira IA, Brandão-Neto J, Medeiros AC. Simvastatin improves the healing of infected skin wounds of rats. *Acta Cir Bras*, 22(Suppl. 1): 57–63 (2007).
- [145] Watts KL, Cottrell E, Hoban PR, Spiteri MA. RhoA signaling modulates cyclin D1 expression in human lung fibroblasts: implications for idiopathic pulmonary fibrosis. *Respir Res*, 88: 1–14 (2006).
- [146] Patel R, Nagueh SF, Tsybouleva N, Abdellatif M, Lutucuta S, Kopelen HA, Quinones MA, Zoghbi WA, Entman ML, Roberts R, Marian AJ. Simvastatin induces regression of cardiac hypertrophy and fibrosis and improves cardiac function in a transgenic rabbit model of human hypertrophic cardiomyopathy. *Circulation*, 104: 317–324 (2001).

- [147] Louneva N, Huaman G, Fertala J, Jiménez SA. Inhibition of systemic sclerosis dermal fibroblast type I collagen production and gene expression by simvastatin. *Arthritis Rheum*, 54: 1298–1308 (2006).
- [148] Meyer-Ter-Vehn T, Katzenberger B, Han H, Grehn F, Schlunck G. Lovastatin inhibits TGF-beta-induced myofibroblast transdifferentiation in human tenon fibroblasts. *Invest Ophthalmol Vis Sci*, 49: 3955–3960 (2008).
- [149] Watts KL, Spiteri MA. Connective tissue growth factor expression and induction by transforming growth factor-beta is abrogated by simvastatin via a Rho signaling mechanism. *Am J Physiol Lung Cell Mol Physiol*, 287: L1323–L1332 (2004).
- [150] Holmes A, Abraham DJ, Sa S, Shi WX, Black CM, Leask A. CTGF and SMADs, maintenance of scleroderma phenotype is independent of SMAD signaling. *J Biol Chem*, 276: 10594–1601 (2001).
- [151] Ko JH, Kim PS, Zhao Y, Hong SJ, Mustoe TA. HMG-CoA reductase inhibitors (Statins) reduce hypertrophic scar formation in a rabbit ear wounding model. *Plast Reconstr Surg*, 129: 252e–261e (2012).
- [152] Stevens DA, Schwartz HJ, Lee JY, Moskovitz BL, Jerome DC, Catanzaro A, Bamberger DM, Weinmann AJ, Tuazon CU, Judson MA, Platts-Mills TA, DeGraff Jr AC. A randomized trial of itraconazole in allergic bronchopulmonary aspergillosis. *N Engl J Med*, 342: 756–762 (2000).
- [153] Al-Shair K, Atherton GT, Harris C, Ratcliffe L, Newton PJ, Denning DW. Long-term antifungal treatment improves health status in patients with chronic pulmonary aspergillosis: a longitudinal analysis. *Clin Infect Dis*, 57: 828–835 (2013).
- [154] Rengasamy M, Chellam J, Ganapati S. Systemic therapy of dermatophytosis: Practical and systematic approach. *Clin Derma Rev*, 1(3): 19–23 (2017).
- [155] Martin MV. The use of fluconazole and itraconazole in the treatment of candida albicans infections: A review. *J Antimicrob Chemother*, 44: 429–437 (2000)

- [156] Schmitt C, Perel Y, Harousseau JL, Lemerle S, Chwetzoff E, le Moing JP, Levron JC. Pharmacokinetics of itraconazole oral solution in neutropenic children during long-term prophylaxis. *Antimicrob Agents Chemother*, 45: 1561–1564 (2001).
- [157] Aftab BT, Dobromilskaya I, Liu JO, Rudin CM. Itraconazole inhibits angiogenesis and tumor growth in non–small cell lung cancer. *Cancer Res*, 71: 6764–6772 (2011).
- [158] Chong CR, Xu J, Lu J, Bhat S, Sullivan DJ, Liu JO. Inhibition of angiogenesis by the antifungal drug itraconazole. *ACS Chem Biol*, 2: 263–70 (2007).
- [159] Mihara M, Hagari Y, Morimura T, Nakayama H, Isihara M, Aki T, Inoue T. Itraconazole as a new treatment for pustulosis palmaris et plantaris. *Arch Dermatol*, 134: 639–640 (1998).
- [160] Bollong MJ, Yang B, Vergani N, Beyer BA, Chin EN, Zambaldo C, Wang D, Chatterjee AK, Lairson LL, Schultz PG. Small molecule-mediated inhibition of myofibroblast transdifferentiation for the treatment of fibrosis. *Proc Natl Acad Sci*, 114: 4679–4684 (2017).
- [161] Okada E, Maruyama Y. Are keloids and hypertrophic scars caused by fungal infection? *Plast Reconstr Surg*, 120: 814–815 (2007).
- [162] Riobo NA, Manning DR. Pathways of signal transduction employed by vertebrate Hedgehogs. *Biochem J*, 403: 369–379 (2007).
- [163] Echelard Y, Epstein DJ, St-Jacques B, Shen L, Mohler J, McMahon JA, McMahon AP. Sonic Hedgehog, a member of a family of putative signaling molecules, is Implicated in the regulation of CNS polarity. *Cell*, 75: 1417–1430 (1993).
- [164] Rohatgi R, Milenkovic L, Scott MP. Patched1 regulates hedgehog signaling at the primary cilium. *Science*, 317: 372–376 (2007).
- [165] Méthot N, Basler K. Suppressor of fused opposes hedgehog signal transduction by impeding nuclear accumulation of the activator form of Cubitus interruptus. *Development*, 127: 4001–4010 (2000).

- [166] Jia J, Tong C, Wang B, Luo L, Jiang J. Hedgehog signaling activity of Smoothened requires phosphorylation by protein kinase A and casein kinase I. *Nature*, 432: 1045–1050 (2004).
- [167] Skoda AM, Simovic D, Karin V, Kardum V, Vranic S, Serman L. The role of the Hedgehog signaling pathway in cancer: A comprehensive review. *Bosn J Basic Med Sci*, 18: 8–20 (2018)
- [168] Gonnissen A, Isebaert S, Haustermans K. Targeting the Hedgehog signaling pathway in cancer: beyond Smoothened. *Oncotarget*, 6: 13899–13913 (2015).
- [169] Sicklick JK, Li YX, Jayaraman A, Kannangai R, Qi Y, Vivekanandan P, Ludlow JW, Owzar K, Chen W, Torbenson MS, Diehl AM. Dysregulation of the Hedgehog pathway in human hepatocarcinogenesis. *Carcinogenesis*, 27: 748–757 (2006).
- [170] Wicking C, Smyth I, Bale A. The hedgehog signaling pathway in tumorigenesis and development. *Oncogene*, 18: 7844–7851 (1999).
- [171] Niyaz M, Khan MS, Mudassar S. Hedgehog signaling: an Achilles' heel in cancer. *Transl Oncol*, 12: 1334–1344 (2019).
- [172] Coon DR, Roberts DJ, Loscertales M, Kradin R. Differential epithelial expression of SHH and FOXF1 in usual and nonspecific interstitial pneumonia. *Exp Mol Pathol*, 80: 119–123 (2006).
- [173] Stewart GA, Hoyne GF, Ahmad SA, Jarman E, Wallace WA, Harrison DJ, Haslett C, Lamb JR, Howie SE. Expression of the developmental Sonic hedgehog (Shh) signaling pathway is upregulated in chronic lung fibrosis and the Shh receptor patched 1 is present in circulating T lymphocytes. *J Pathol*, 199: 488–495 (2003).
- [174] Hu B, Wu Z, Bai D, Liu J, Liu T, Phan SH. Targeting the Hedgehog signaling pathway as therapy for pulmonary fibrosis. *Am J Respir Crit Care Med*, 193: A2421 (2016).
- [175] Shen J, Yan J, Wei X, Liu Z, Jin L. Gant61 ameliorates CCl4-induced liver fibrosis by inhibition of Hedgehog signaling activity. *Toxicol Appl Pharmacol*, 387: 114853 (2020).

- [176] Greenbaum LE. Hedgehog signaling in biliary fibrosis. *J Clin Invest*, 118: 3263–3265 (2008).
- [177] Fabian SL, Penchev RR, St-Jacques B, Rao AN, Sipilä P, West KA, McMahon AP, Humphreys BD. Hedgehog-Gli pathway activation during kidney fibrosis. *Am J Pathol*, 180: 1441–1453 (2012).
- [178] Horn A, Palumbo K, Cordazzo C, Dees C, Akhmetshina A, Tomcik M, Zerr P, Avouac J, Gusinde J, Zwerina J, Roudaut H, Traiffort E, Ruat M, Distler O, Schett G, Distler JHW. Hedgehog signaling controls fibroblast activation and tissue fibrosis in systemic sclerosis. *Arthritis Rheum*, 64: 2724–2733 (2012).
- [179] Luchetti G, Sircar R, Kong JH, Nachtergaelle S, Sagner A, Byrne EFX, Covey DF, Siebold C, Rohatgi R. Cholesterol activates the G-protein coupled receptor Smoothened to promote Hedgehog signaling. *eLife*, 5: e20304 (2016).
- [180] Huang P, Nedelcu D, Watanabe M, Jao C, Kim Y, Liu J, Salic A. Cellular cholesterol directly activates smoothened in Hedgehog signaling. *Cell*, 166: 1176–1187 (2016).
- [181] Deshpande I, Liang J, Hedeen D, Roberts KJ, Zhang Y, Ha B, Latorraca NR, Faust B, Dror RO, Beachy PA, Myers BR, Manglik A. Smoothened stimulation by membrane sterols drives Hedgehog pathway activity. *Nature*, 571: 284–288 (2019).
- [182] Kim J, Tang JY, Gong R, Kim J, Lee JJ, Clemons KV, Chong CR, Chang KS, Fereshteh M, Gardner D, Reya T, Liu JO, Epstein EH, Stevens DA, Beachy PA. Itraconazole, a commonly used antifungal that inhibits Hedgehog pathway activity and cancer growth. *Cancer Cell*, 17: 388–399 (2010).
- [183] Ueda T, Tsubamoto H, Inoue K, Sakata K, Shibahara H, Sonoda T. Itraconazole modulates hedgehog, WNT/β-catenin, as well as akt signaling, and inhibits proliferation of cervical cancer cells. *Anticancer Res*, 37: 3521–3526 (2017).
- [184] Hu Q, Hou YC, Huang J, Fang JY, Xiong H. Itraconazole induces apoptosis and cell cycle arrest via inhibiting Hedgehog signalling in gastric cancer cells. *J Exp Clin Cancer Res*, 36: 50–61 (2017).

- [185] Kim JS, Cho KS, Park SH, Lee SH, Lee JH, Jeong KH, Lee TW. Itraconazole attenuates peritoneal fibrosis through its effect on the sonic hedgehog signaling pathway in mice. *Am J Nephrol*, 48: 456–464 (2018).
- [186] Tsai YC, Tsai TF. Itraconazole in the treatment of nonfungal cutaneous diseases: A review. *Dermatol Ther (Heidelb)*, 9: 271–280 (2019).

## **VIII. Acknowledgement**

First of all, I would like to express my deep appreciation to my supervisor, Professor Dr. Dr. h.c. E. Märtilbauer, for offering me the opportunity to study in the Chair for Hygiene and Technology of Milk. This work would not be successfully completed without his full support, excellent guidance, and insightful comments.

Then, I wish to show my gratitude to my second supervisor, Dr. Yuval Rinkevich for walking me through the path of my PhD study. Due to his insightful suggestions and patient guidance, this thesis could be finally presented. I am impressed by his fantastic scientific thinking, rigorous research attitude, and profound knowledge.

I would also like to pay my special regards to Dr. Andrea Didier and Mrs. Maria Wittmann for their kind suggestions, academic input and text-editing efforts in accomplishing this thesis.

Sincere thanks to Dr. Tim Koopmans for his smart advices and encouragement. I have benefited a lot at both academic and personal level.

I also take this opportunity to give my thanks to Mrs. Sandra Schiener. I appreciate her for helping me take care of many official documents and for her encouragement during my study.

I also give my thanks to all the members of the Chair for Hygiene and Technology of Milk and all lab members from Dr. Rinkevich's group, with whom I have spent an unforgettable time in a favourable atmosphere.

I am deeply indebted to my motherland- People's Republic of China and the China Scholarship Council for providing me the chance and financial support to study in Germany.

Lastly, big thanks go to my family in China, who supported me with their selfless love and helped me to go through all the hard times during my PhD study.